Taylor & Francis
Taylor & Francis Group

RESEARCH PAPER

TssI2-TsiI2 of *Vibrio fluvialis* VflT6SS2 delivers pesticin domain-containing periplasmic toxin and cognate immunity that modulates bacterial competitiveness

Yuanming Huang, Yu Han, Zhenpeng Li, Xiaorui Li, Zhe Li, Ping Liu, Xiaoshu Liu, Qian Cheng, Fenxia Fan, Biao Kan, and Weili Liang

State Key Laboratory of Infectious Disease Prevention and Control, National Institute for Communicable Disease Control and Prevention, Chinese Center for Disease Control and Prevention, Beijing, China

ABSTRACT

Vibrio fluvialis is a halophilic Gram-negative bacterium regarded as an emerging unusual enteric pathogen of increasing public health concern. Our previous work has identified two type VI secretion systems (T6SSs) in *V. fluvialis*, VflT6SS1, and VflT6SS2, and the latter is functional in mediating interbacterial competitiveness. However, its antibacterial effectors remain to be clarified. In this work, we focused on a new potential effector/immunity pair TssI2/TsiI2. Bioinformatics analysis revealed that the C-terminal domain of TssI2 belongs to a widespread family of pesticin, and its antibacterial toxicity and corresponding protection by TsiI2 were proved via bacterial killing assays, and their action sites were localized to the periplasm of bacterial cells. The interaction of TssI2 and TsiI2 was demonstrated by the bacterial adenylate cyclase two-hybrid, protein pull-down and isothermal titration calorimetry assays. Site-directed mutagenesis demonstrated that, in addition to Glu-844, Thr-863, and Asp-869, which correspond to three reported residues in pesticin of *Yersinia pestis*, additional residues including Phe-837, Gly-845, Tyr-851, Gly-867, Gln-963, Trp-975, and Arg-1000 were also proved to be crucial to the bactericidal activity of TssI2. Muramidase/lysozyme-related peptidoglycan (PG) hydrolase activities of TssI2 and its variants were validated with permeabilized *Escherichia coli* cells and purified PG substrate. Based on sequence homologies at C-terminals in various *V. fluvialis* isolates, TssI2 was subdivided into five clusters (12–22% identity among them), and the antibacterial activities of representative effectors from other four Clusters were also confirmed through periplasmic over-expression in *E. coli* host. Two selected cognate immunities were proved to confer protection against the toxicities of their effectors. Additionally, TsiI2, which belongs to Cluster I, exhibited cross-protection to effector from Cluster V. Together, current findings expand our knowledge of the diversity and consistency of evolved VgrG effectors in *V. fluvialis* and on how VflT6SS2 mediates a competitive advantage to gain a better survival.

Introduction

Type VI secretion system (T6SS) is a nanoweapon widely used by Gram-negative bacteria to deliver toxic effectors into antagonizing competitors to gain a competitive fitness advantage.[1,2] The T6SS comprises 13–14 "core" components, which assemble into the basal complex, the membrane complex, the sheath components, and the puncturing device.[3,4] The formation of the membrane complex TssJLM initiates the assembly of T6SS,[5–7] then recruits the TssEFGK basal complex built around a central VgrG-PAAR spike,[8] followed by TssA connecting the basal complex to the Hcp tube encased within an outer TssBC sheath component. The contraction of sheath components propels the Hcp-VgrG-PAAR puncturing device and translocates Hcp, VgrG, and associated effectors into neighbor target cells.[9] The T6SS apparatus shares a common evolutionary origin with phage tail-associated protein complexes[10] and a common assembly pathway with bacteriophage tail tubes.[11] The T6SS operates via dynamic cycles of assembly, contraction, and disassembly. In terms of protein transport across lipid membrane to neighbor cells, the T6SS is very efficient.[12,13] Although the T6SS can deliver effector proteins into an eukaryotic or fungal cell,[14,15] and has even been proposed to mediate ion transport,[16] the function of most

T6SS effector proteins is still associated with antibacterial activity.[17]

The T6SS effectors can be classified as either cargo effectors or specialized effectors based on their transport mechanisms.[1] The cargo effector is a protein with particular enzyme activity. It requires or not an adaptor or dedicated chaperone protein to load onto one of the components of the tail spike structure (Hcp, PAAR, or VgrG) for delivery purposes.[18] The DUF4123, DUF1795, DUF1875, and DUF2169 domains are usually found in the T6SS adaptors or chaperone proteins.[19–22] In contrast, the specialized effector is the homolog of one of these tail spike components that contain an additional effector domain covalently fused to the core domain, usually in the C-terminus of Hcp, VgrG, or PAAR.[13,21,23–25] These covalent fusions function not only as of the structural components of the T6SS apparatus but also as the secreted effector proteins. Specialized Hcps with diverse C-terminal toxic domains were recently found in the Enterobacteriaceae.[25] Specialized PAAR and VgrG effectors are widespread, and many different examples have been reported, including the diverse Rhs family proteins.[21,26] The specialized VgrG effectors are also termed as "evolved VgrG" which contains a C-terminal extension covalently fused to the gp5 and gp27-like core region of VgrG,[26,27] such as VgrG-1 and VgrG-3 from *V. cholerae*, each containing actin cross-linking domain and peptidoglycan (PG) glycoside hydrolase domain.[13,23,28] It is also found that certain C-terminal extensions of VgrGs do not confer toxic functions per se but bind and recruit other effectors.[29–31] To date, various antibacterial effectors and many "trans-kingdom" effectors acting on both prokaryotic and eukaryotic cells have been identified with diverse enzymatic activities, including nucleases, lipase, lysozymes, and so on.[32–36]

V. fluvialis is a halophilic Gram-negative bacterium that is commonly found in coastal environments.[37] It causes sporadic cases and outbreaks of cholera-like bloody diarrhea and various extraintestinal infections with primary septicemia in immunocompromised individuals.

Thus, it is considered as an emerging foodborne pathogen causing increasing public health concern, especially considering the rising prevalence of *V. fluvialis* infection[37] and the increasing incidence of multidrug-resistant isolates.[38–41] Previously, we characterized two T6SS gene clusters (VflT6SS1 and VflT6SS2) in a *V. fluvialis* clinical isolate 85003. The activity of VflT6SS1 is not detected under normal laboratory culture conditions, but VflT6SS2 is active under low (25°C) and warm (30°C) temperatures and mediates antibacterial activity and can be activated by high osmolarity conditions at 37°C, a nonpermissive temperature at which VflT6SS2 is inert under normal culture condition.[42] The transcription and function of VflT6SS2 is regulated by the integration host factor (IHF) and CqsA/LuxS-HapR quorum sensing system.[43,44] However, the effector proteins that contribute to the antibacterial activity of VflT6SS2 have not been described yet.

This study reported a new VgrG effector, TssI2, in the VflT6SS2 major cluster, which contains a pesticin (Pst) domain at the C-terminal. We demonstrated that this Pst domain-containing C-terminal fragment accounts for the antibacterial activity of TssI2, meanwhile its downstream TsiI2 functions as a cognate immunity through physical interaction. We also revealed that TssI2 has muramidase/lysozyme activity by cleaving the β-1,4-glycosidic bond of PG molecule and the Pst domain-containing proteins exist widely in various module combination structures, with the most abundance in γ-proteobacteria. Furthermore, we identified additional residues vital to the antibacterial activity and PG hydrolase activity of TssI2. Based on sequence homologies, five clusters of C-terminal extensions in evolved VgrGs were established from dozens of *V. fluvialis* isolates. Although sharing low sequence identity among the clusters, representative from each of them all displayed intense bactericidal activity. Besides the protective effect endowed by immunity against its cognate effector, cross-protection to non-cognate effector was also identified. Together, this study

broadened our understanding of the diversity and functional mechanism of evolved VgrG effectors and their cognate immunities.

Results

### TssI2-TsiI2 is a new VflT6SS2 antibacterial effector-immunity pair

Our previous study has shown that VflT6SS2 is functionally expressed in *V. fluvialis* 85003 and associated with antibacterial activity.[42] TssI2 is a 1012-amino-acid VgrG protein encoded at the end of the VflT6SS2 major cluster, which has highly conserved genetic contents and gene organization with those of *Vibrio cholerae* T6SS[42] (Figure 1a). VgrG3 (VCA0123), the homolog of TssI2 in *V. cholerae*, has a hydrolase activity and degrades PG in the periplasm of target bacteria,[32] and its following gene VCA0124 encodes the immunity protein against VgrG3.[23] However, sequence alignment of TssI2 and VgrG3 revealed that though TssI2 residues 1–829 had 67% sequence identity to VgrG3 residues 1–811, their remaining C-terminal regions and the downstream genes had no homologies (Figure 1a), suggesting that TssI2 might be a novel extension domain-containing VgrG effector in *V. fluvialis* and the downstream TsiI2 is the potential immunity of TssI2.

To test whether TssI2 and TsiI2 are VflT6SS2 effector-immunity pairs, we constructed the ΔtssI2 and ΔtssI2-tsiI2 mutants of *V. fluvialis*. Mutants ΔvasH[42] and ΔvasK (this mutant will be described elsewhere) were used as T6SS negative controls. The bacterial killing assay with *E. coli* MG1655 as prey showed that the wild-type *V. fluvialis* could strongly inhibit the survival of MG1655 after 5 h co-incubation, but this ability was significantly impaired in ΔtssI2 mutant though the degree was not as strong as ΔvasH mutant where the VflT6SS2 completely lost its capability due to depleted expression of Hcp, the key structural component of T6SS inner tube[42] (Figure 1b). This observation suggests that TssI2 contributes to the antibacterial virulence mediated by VflT6SS2 in *V. fluvialis*. To exclude the possibility that the defect of

ΔtssI2 antibacterial activity was an indirect effect caused by somehow reduced secretion function of VflT6SS2, we measured the Hcp secretion in ΔtssI2 mutant with and without MG1655 co-culture. Western blot analysis showed that the deletion of *tssI2* did not affect the expression and secretion of Hcp (Figure 1c), indicating that the antibacterial virulence defect of ΔtssI2 is due to the deficiency of the effector per se. To further evaluate the bactericidal ability of TssI2, we performed the self-intoxication assay using the ΔtssI2-tsiI2 double mutant as prey. As shown in Figure 1d, only the wild-type strain repressed the growth of the prey, while both ΔtssI2 and ΔtssI2-tsiI2 failed to kill the ΔtssI2-tsiI2 mutant, and the situation is similar to ΔvasK mutant where T6SS is nonfunctional. To exclude the possibility of *tssI2* gene mutation polarity, we performed complementation test. As shown in Figure 1e, the complementation of ΔtssI2 mutant with an inducible TssI2-expressing plasmid pTssI2 greatly recovered the ability of ΔtssI2 to compete against the ΔtssI2-tsiI2 mutant compared with control vector pSRKTc. These results established that TssI2 had the bactericidal ability, and the lack of *tsiI2* in ΔtssI2-tsiI2 resulted in the loss of protection against TssI2-mediated self-intoxication, indicating that TsiI2 is the immune protein of TssI2 effector. Consistently, introducing a complement plasmid pTsiI2 into ΔtssI2-tsiI2 mutant significantly increased the survival of the prey compared to pSRKTc vector control, further confirming that TsiI2 is the cognate immunity of TssI2 (Figure 1f). We noticed that WT *V. fluvialis* showed higher killing ability with *E. coli* MG1655 as prey (Figure 1b) than with ΔtssI2-tsiI2 (Figure 1d). To exclude the possibility that TssI2 expression was differently induced with interaction with prey, we measured the *tssI2* mRNA abundance without and with different prey species. No obvious differential expression of *tssI2* was detected by quantitative real-time PCR analysis under different prey conditions (data not shown). Therefore, the difference of WT killing ability to MG1655 and ΔtssI2-tsiI2 preys is probably due to the existence of multiple bactericidal effectors besides TssI2 in *V. fluvialis*. Despite ΔtssI2-tsiI2 prey is devoid
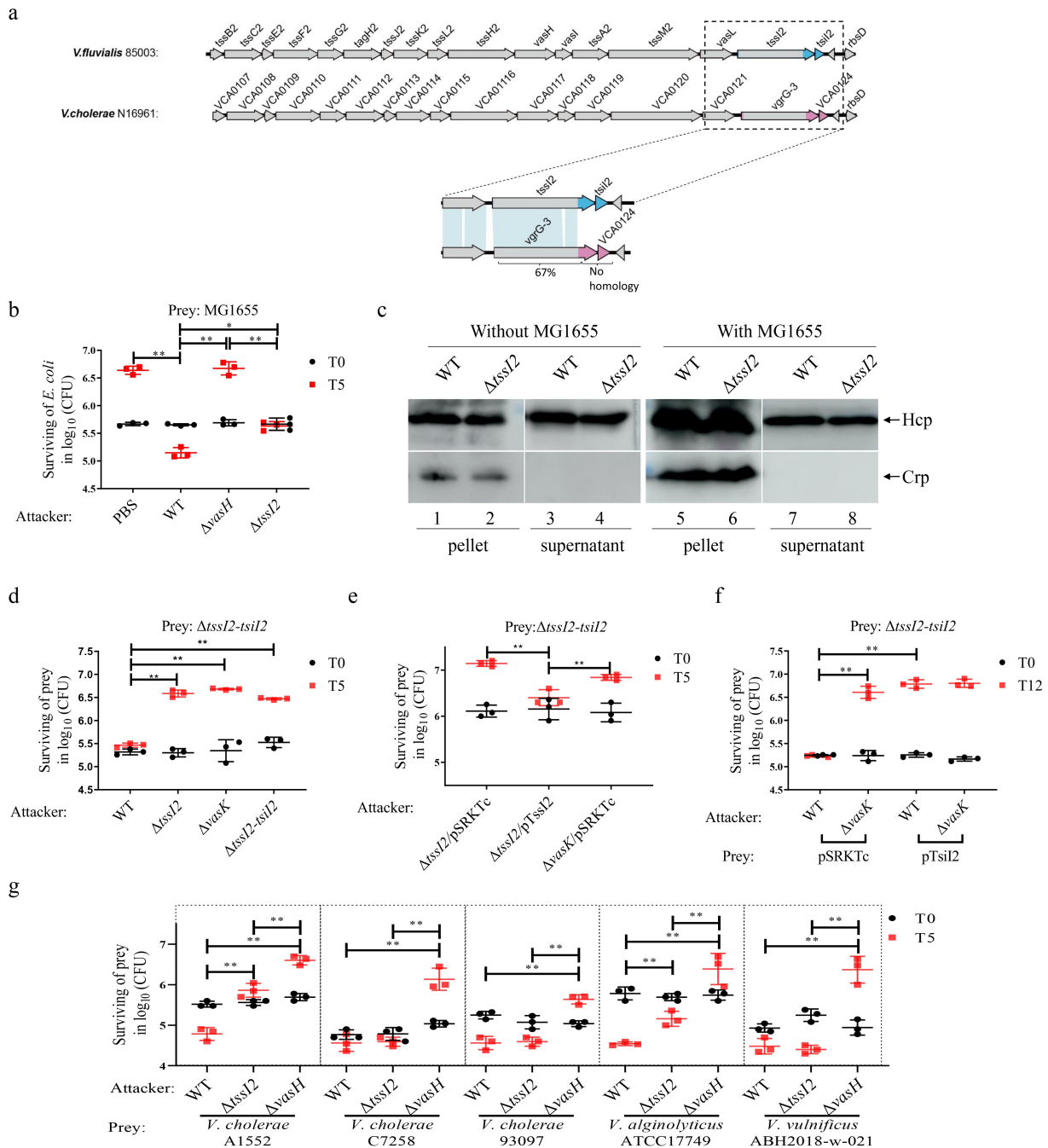
Figure 1. TssI2-Tsil2 is an antibacterial effector-immunity pair. (a) Genetic organization of VflT6SS2 major cluster of *V. fluvialis* 85003 and that of T6SS major cluster of *V. cholerae* N16961 and homology comparison of their 3′ end. (b) Viability counts of *E. coli* MG1655 prey before (0 h) and after (5 h) co-incubation with phosphate buffered solution (PBS) or the indicated *V. fluvialis* 85003 attackers on media containing 340 mM NaCl at 30°C. PBS was used as blank control, and wild type (WT) was used as T6SS⁺ while ΔvasH as T6SS⁻ controls. Statistical analysis was performed by one-way ANOVA with Dunnett's T3 test using the surviving *E. coli* MG1655 between samples at 5 h time point (*$P < .05$, **$P < .01$). (c) Western Blot analysis of Hcp expression in WT and Δtssl2 mutant co-cultured with and without prey MG1655. Cell pellets and culture supernatants were analyzed by immunoblot assays using anti-Hcp and anti-Crp antibodies. Lanes 1–2 and 5–6, cell pellets; lanes 3–4 and 7–8, culture supernatants. The arrows indicate the reaction bands of the Hcp and Crp proteins. (d) (e) (f) Viability counts of Δtssl2-tsil2 prey or Δtssl2-tsil2 containing complement plasmid pTsil2 or pSRKTc empty vector before (0 h) and after (5 h or 12 h) co-incubation with the indicated *V. fluvialis* 85003 attackers on media containing 340 mM NaCl at 30°C. WT was used as T6SS⁺, and ΔvasK or ΔvasK/pSRKTc as T6SS⁻. The Δtssl2/pTssl2 was used as tssl2 tran-complemented strain. Statistical analysis was performed by one-way ANOVA with Dunnett's T3 test using the surviving prey between samples at 5 h or 12 h time point (**$P < .01$). (g) Viability counts of *V. cholerae* toxigenic strains A1552 and C7258, nontoxigenic strain 93097, *V. alginolyticus* ATCC17749 and *V. vulnificus* ABH2018-w-021 before (0 h) and after 5 h co-incubation with *V. fluvialis* 85003 attackers on media containing 340 mM NaCl at 30°C. WT was used as T6SS⁺, and ΔvasH as T6SS⁻. Statistical analysis was performed by one-way ANOVA with Dunnett's T3 test using the surviving prey between samples at 5 h time point (**$P < .01$).
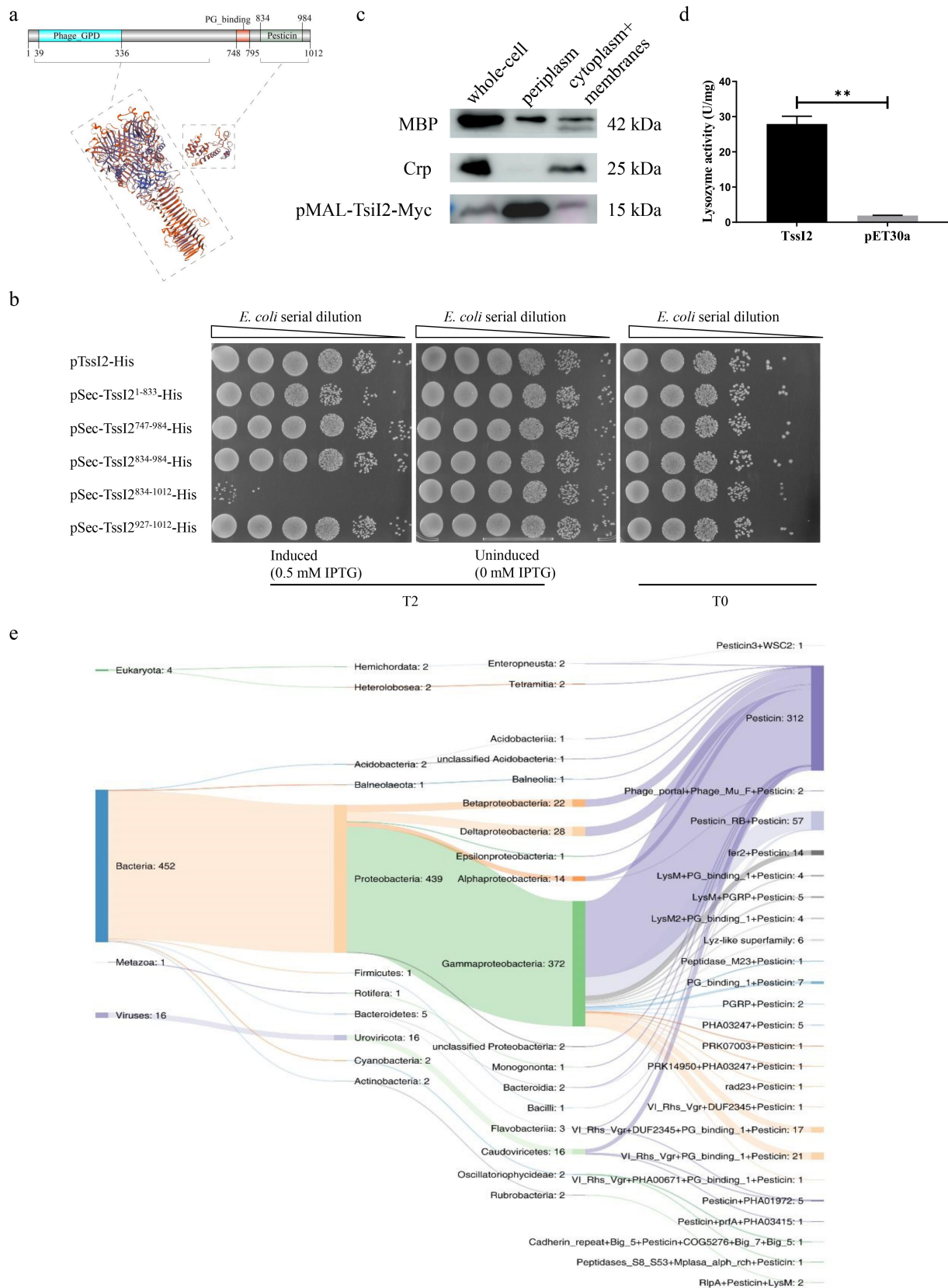
Figure 2. Functional domain characterization and taxonomic distribution analysis of TssI2 C-terminal domain. (a) Schematic representation of the domain architecture of TssI2 protein. The atomic model shows the results of the Swiss-MODEL prediction of TssI2 N-terminal residues 13–627 and C-terminal residues 834–1010 reference to templates 6h3n.1.B and 4AQN.1.B respectively. (b) Bactericidal activities of TssI2 and its various truncated constructs in *E. coli* MG1655. *E. coli* MG1655 transformants containing the

of *tssI2*, it contains other possible effector-immunity pairs, and the inhibition on T6SS-negative MG1655 is the synergistic effect of multiple effectors while that on Δ*tssI2-tsiI2* only comes from TssI2 effector. Consistent to this speculation, when Δ*tssI2* was used as attacker, it could still partially inhibit proliferation of MG1655 (Figure 1b) but not Δ*tssI2-tsiI2* (Figure 1d), though the inhibition extent is significantly lower than that of WT but obviously higher than Δ*vasH* (Figure 1b). Altogether, these data demonstrated that TssI2-TsiI2 is an effector-immunity pair involved in VflT6SS2-mediated antibacterial virulence in *V. fluvialis*.

Additionally, we investigated the VflT6SS2 and TssI2 mediated antibacterial effect against other pathogenic *Vibrio* species, including toxigenic and non-toxigenic *V. cholerae, V. alginolyticus*, and *V. vulnificus*, which share a common aquatic environment with *V. fluvialis*. The bacterial killing assays showed that wild-type *V. fluvialis* could inhibit the growth of all tested-preys with varying degrees comparing to Δ*vasH* mutant whose VflT6SS2 is loss of function, while TssI2 seems only partially contribute to the killing ability of *V. fluvialis* against toxigenic *V. cholerae* A1552 and *V. alginolyticus* ATCC17749 but have no inhibitory effect to *V. cholerae* toxigenic strain C7258, non-toxigenic strain 93097, and *V. vulnificus* ABH2018-w-021 (Figure 1g). These results further illustrated that VflT6SS2 could endow *V. fluvialis* a survival advantage by inhibiting other species competing for a common niche and its TssI2 effector mediated bactericidal activity displays species- and/or strain-specific effect.

TssI2 belongs to a widespread family of pesticin

To further investigate the bactericidal activity and structural characteristics of TssI2, we firstly performed conserved domain prediction by searching the Pfam[45] and SWISS-MODEL[46] databases. The Pfam predicted that the N-terminal of TssI2 possesses a Phage_GPD domain (residues 39–336), and the C-terminal contains two domains: a PG_binding domain (residues 748–795) and a Pst domain (residues 834–984). SWISS-MODEL analysis also revealed that the N-terminal of TssI2 (residues 13–627) shares 35.52% identity with VgrG1 protein (template 6h3n.1.B), and the C-terminal (residues 834–1010) shares 29.78% identity with *Yersinia pestis*'s Pst (PDB code 4AQN.1.B). These analyses indicated that TssI2 is an evolved VgrG harboring a C-terminal Pst extension (Figure 2a).

Since Pst is a bacteriocin protein toxin produced by *Y. pestis* to kill related bacteria of the same niche and confers muramidase/lysozyme activity in the periplasm,[47] we reasoned that TssI2 might also target the cell wall and function in the periplasmic space. To verify the hypothesis and dissect the related functional domain, we constructed a series of recombinant plasmids expressing the full-length TssI2 and its different truncates. These plasmids were introduced into *E. coli* MG1655 to measure their bactericidal activities. As expected, cytoplasmic expression of full-length TssI2 (pTssI2-His) displayed no killing effect. Unexpectedly, we tried but could not get the full-length *tssI2* construct with Sec signal peptide fusion. We inferred that this might be due to the toxicity of expression of TssI2 in the periplasm. Among the truncated

---

indicated constructs were normalized to 3.5 McF, 1:100 diluted in 5 ml LB and incubated at 37°C for 1 h (T0). Then the culture was split in two, one half was induced by adding IPTG, and the other half was used as a control. The cultures were continually incubated for 2 h (T2). 10-fold serial dilutions were spotted on gentamicin-resistance LB agar at T0 and T2 time points. (c) Cells of *V. fluvialis* Δ*tssI2-tsiI2* mutant expressing pMAL-TsiI2-Myc were fractionated and analyzed by Western blotting using anti-Myc, anti-Crp (cytoplasmic), and anti-MBP (periplasm) antibodies. (d) Lysozyme activity detection of purified TsiI2 protein *in vitro*. The *tssI2* gene was cloned into the pET-30a(+) vector with a C-terminal His-tag, expressed in BL21(DE3)pLysS with IPTG induction. The purified His-TsiI2 was assayed for lysozyme activity using the fluorescence-labeled *M. lysodeikticus* substrate. The supernatant of empty pET-30a(+) vector was used as a negative control. Statistical analysis was performed by unpaired T test using the lysozyme activity between purified His-TsiI2 and empty pET-30a(+) vector (**$P < .01$). (e) Illustration of the distribution of the pesticin domain in various microbe species. A Sankey diagram depicted the relationship between bacterial taxa (kingdom, phylum, and class from left to right) and various proteins harboring pesticin domains (rightmost). The types of composition domains and multidomain architectures of target proteins were shown. The number of sequences involved in each node was labeled after the name of taxon or type of domains.
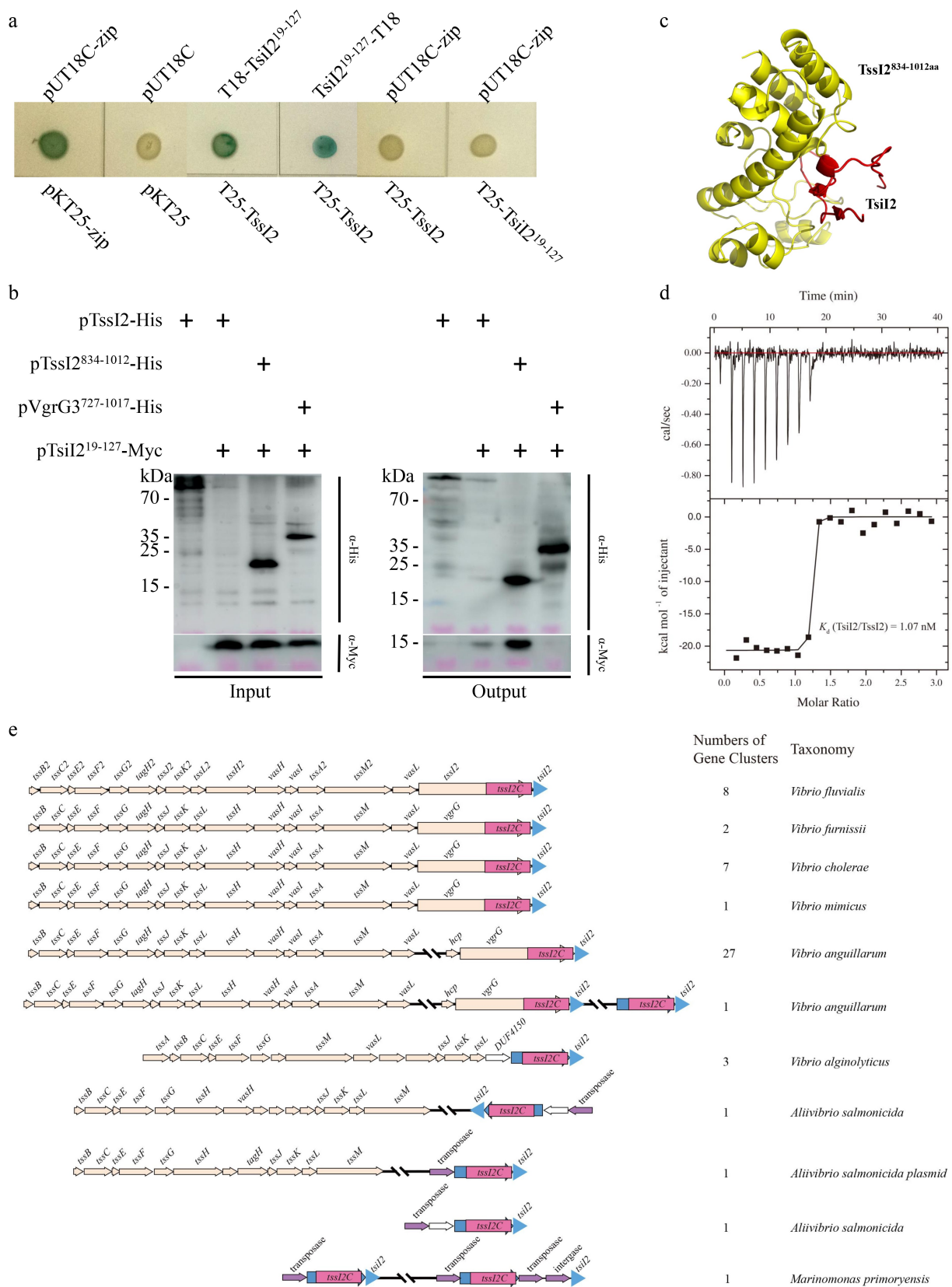
Figure 3. Characterization of the interaction between TsiI2 and TssI2. (a) Bacterial two-hybrid analysis of TssI2–TsiI2 interaction. pT25-TssI2 and pT18-TsiI2$^{19–127}$ or pTsiI2$^{19–127}$-T18 constructs expressing the indicated proteins fused in frame to the T25 or T18 domain of the *B. pertussis* adenylate cyclase were co-expressed in the reporter strain BTH101 on LB agar supplemented with IPTG and X-gal. The pKT25-zip and pUT18C-zip served as positive control, pUT18C and pKT25 as negative control, and pUT18C-zip and T25-TssI2 or T25-

constructs with Sec fusion, pSec-TssI2$^{834-1012}$-His includes the predicted Pst domain (residues 834–984) as well as the last 28 C-terminal residues readily killed *E. coli* host. The constructs expressing the TssI2 N-terminal 833 residues (pSec-TssI2$^{1-833}$-His), the PG binding and Pst domain (pSec-TssI2$^{747-984}$-His), the Pst domain alone (pSec-TssI2$^{834-984}$-His), or the C-terminal 86 residues (pSec-TssI2$^{927-1012}$-His) did not show apparent antibacterial activity. These results demonstrated that the C-terminal 179 residues covering the Pst domain (residues 834–984) and the last C-terminal 28 residues are required for TssI2 antibacterial activity when located in the periplasmic space of *E. coli* (Figure 2b and S1). The above results also indicate that the major destination for incoming TssI2 is likely to be the periplasm of target cells. Consistently, immunity TsiI2 was supposed to be at periplasmic space as a Sec peptide was predicted at its N-terminal. For further confirmation, we performed subcellular fractionation of *V. fluvialis* Δ*tssI2-tsiI2* mutant cells expressing pMAL-TsiI2-Myc isolating whole cells, periplasmic contents, and the membrane/cytosolic fraction and assayed for the presence of TsiI2. The results clearly showed that the Myc-tagged TsiI2 protein was mainly detected in the periplasmic section (Figure 2c), implying that TsiI2 interacts with TssI2 in the periplasm of *V. fluvialis*. Subsequently, we cloned and purified the TssI2 with a C-terminal 6× His tag. The hydrolase activity of the purified TssI2 protein was assayed *in vitro* using fluorescence-labeled *Micrococcus lysodeikticus* cell walls as a substrate according to the manufacturer's directions (Thermo Fisher Scientific). The result demonstrated that the TssI2 protein induced a 14.5-fold increment of enzymatic activity compared with its empty vector indicating it has a lysozyme activity (Figure 2d).

To further dissect the sequence feature, we used position-specific iterated BLAST (PSI-BLAST) to search for the homologs of the TssI2 C-terminal region in the non-redundant protein database of NCBI (Dec 31, 2020), and a total of 473 proteins containing a Pst domain (Supplementary Data 1) were identified. These proteins are annotated at the class level, 439 of which belong to Proteobacteria, including γ-Proteobacteria (84.74%), δ-Proteobacteria (6.38%), and β-Proteobacteria (5.01%). Interestingly, 16 homology proteins come from the class Caudoviricetes in the viruses. The Pfam results showed that 65.96% of the 473 homologous proteins contain only the Pst domain, and the rest of the proteins carry additional domain(s) with distinct predicted functions. Twenty-five different modular genetic combination forms were identified. Forty proteins possess the predicted VI_Rhs-Vgr domain indicating their association with T6SS, 21 of which show similar domain organization as TssI2 where the Pst domain fused to the PG_binding domain and Phg_GPD domain (Figure 2e), and another 18 proteins carry an additional DUF2345 domain that is considered to extend the T6SS spike in Enteroaggregative *E. coli*[31] and exert antibacterial and antifungal effect itself in *Klebsiella pneumoniae*.[48] Together, these results showed that TssI2 possesses cell wall hydrolase activity, and its C-terminal region is functional and belongs to the Pst family, which is widespread in the class γ-Proteobacteria.

TssI2 interacts with TsiI2

As immunity of the TssI2 effector, TsiI2 is located downstream of and adjacent to TssI2 and efficiently

---

TsiI2$^{19-127}$ as specificity controls. (b) Pull-down assay of the interaction of TsiI2$^{19-127}$ with full-length TssI2 or its C-terminal region. The His-tagged TssI2 or TssI2$^{834-1012}$ (TssI2 C-terminal) was co-expressed with Myc-tagged TsiI2$^{19-127}$ in *E. coli* BL21(DE3). Cell lysates were incubated with HisPur™ Ni-NTA resin, and bound proteins were analyzed by Western blotting using anti-His and anti-Myc monoclonal antibodies. Co-expression of His-tagged VgrG3$^{727-1017}$ and Myc-tagged TsiI2$^{19-127}$ was used as a negative control. (c) Model of the predicted TsiI2 C-terminal domain binding to TsiI2 protein based on ZDOCK prediction, with TssI2 C domain depicted in yellow, and TsiI2 labeled in red. (d) ITC analysis of specific binding between TssI2 and TsiI2. Purified TssI2 (15 μM) was titrated with purified TsiI2$^{19-127}$ (210 μM), TsiI binds to TssI2 with a K_d of 1.07 nM. Top panel shows the raw calorimetric data for the interaction, and bottom panel shows the integrated heat variation, corrected for dilution heat, to fit the "one set of sites binding model". (e) Diagram of the co-occurrence of TssI2 C-terminal and TsiI2 in 53 gene clusters from tBLASTn search. The T6SS structure genes are colored in apricot, the homologs of TssI2 C-terminal, TsiI2, and transposase/integrase are in pink, blue and purple, respectively.

Figure 4. Exploration of key residues responsible for TssI2 C-terminal activity. (a) Schematic of the conserved domains and homology alignment of *Y. pestis* pesticin and TssI2. (b) The amino acid sequence alignment of TssI2 C-terminal and *Y. pestis* pesticin. The identical residues are highlighted in red. Residues chosen for alanine substitutions are marked with arrows. The most critical residues resulting in complete loss of activity in both pesticin and TssI2 are indicated with red arrows, and the less critical residues with Orange arrows. (c) The structure alignment of TssI2 C-terminal (residues 834–1012) (left) and Pst^A (residues 167–357) of *Y. pestis* pesticin (PDB code 4AQN) (right) in ribbon representation. Residues mutated according to the sequence and structure alignment are represented as sticks together with residue and number for both TssI2 and pesticin. (d) (g) Survival of *E. coli* expressing wild type TssI2 C-terminal or its variants containing substitutions of alanine for selected residues. The bacterial lawns containing the indicated constructs were normalized to 3.5 McF, 1:100 diluted in LB and incubated at 37°C for 1 h (T0). Then the culture was divided in half. One half was induced by adding IPTG, and the other half was not induced as a control. The cultures were continually incubated for 2 h (T2). 10-fold serial dilutions of cultures were spotted on LB agar. (e) Schematic diagram of TssI2 C-terminal three-dimensional structure. The red pocket in the upper-left panel was predicted by CASTp 3.0 server. The right panel shows a zoom-in into the structure with the residues selected for alanine substitutions are represented as sticks together with residue and number. The residues in dashed box are mutated ones selected according to the sequence alignment of 473 Pst domain containing proteins. Two components forming the activity domain of TssI2 are encircled by dotted lines. (f) Weblogo depicting conserved residues of TssI2 C-terminal sequences derived from the alignment of 473 Pst domain containing homologs. Red arrows indicate the conserved residues that are mutated in current and previous studies,[52] while dashed boxes indicate the newly selected residues for alanine substitutions in this study.

restrained the TssI2-mediated self-toxication in *V. fluvialis* 85003 (Figure 1f). Besides, TssI2 exerted the antibacterial effect in periplasm (Figure 2b) meanwhile TsiI2 was proved to be located in the periplasmic space (Figure 2c). The functional association and the consistent spatial co-localization of

TsiI2 and TssI2 imply the possibility of interaction between each other. To verify this speculation, we used a bacterial two-hybrid system based on the functional complementation of T18 and T25 fragments of *Bordetella pertussis* adenylate cyclase.[49] The interacting proteins functionally reconstitute

the activity of adenylate cyclase that results in a Cya + phenotype, i.e. blue colony on LB agar supplemented with X-gal. Thus, *tssI2* was cloned in pKT25 at the C-terminal of the T25 polypeptide and *tsiI2* without N-terminal Sec-secretion signal sequence into pUT18C, pUT18, or pKT25. We observed Cya+ phenotype when T25-TssI2 was co-expressed with either T18-TsiI2$^{19-127}$ or TsiI2$^{19-127}$-T18, but no Cya+ phenotype between T18-zip and T25-TssI2 or T25-TsiI2$^{19-127}$, suggesting a specific interaction between TssI2 and TsiI2 (Figure 3a). Subsequently, we performed a protein pull-down assay to further confirm the interaction, and our results demonstrated that full-length TssI2 or its C-terminal interacted with TsiI2. In contrast, the negative control protein VgrG3$^{727-1017}$ of *V. choleare* could not interact with TsiI2 (Figure 3b). Furthermore, based on the 3D model of TssI2 C-terminal residues 834–1012 and TsiI2 predicted by SWISS-MODEL and Alphafold2,[50] we built the protein docking model of TssI2 C-terminal and TsiI2 by using the ZDOCK service.[51] The generated model suggested that TsiI2 directly binds TssI2 C-terminal by inserting itself into the groove of the TssI2 C-terminal domain (Figure 3c and Table S1). We further examined the interaction intensity between TssI2 and TsiI2 by isothermal titration calorimetry (ITC) analysis and the result revealed a very strong binding affinity between TssI2 and TsiI2 with a disassociation constant (K_d) of 1.07 nM (Figure 3d and S2).

By using tBLASTn, we searched the co-occurrence of TssI2 C-terminal and TsiI2 protein in the non-redundant database of NCBI (Jun 11, 2021). We got 55 hits from 53 gene clusters in 52 strains, which all belong to marine bacteria, including *Marinomonas, Aliivibrio*, and *Vibrio* (Figure 3e and Supplementary Data 2). The TssI2 C-terminal and TsiI2 mainly coexist as modules flanking the structural gene cluster or in the accessory cluster of T6SS. Specifically, in *V. fluvialis, V. furnissii, V. cholerae*, and *V. mimicus*, these genetic modules are located at the 3' end of the T6SS major cluster. While in the hits from *V. anguillarum*, the module is located in the *hcp-vgrG* accessory cluster of T6SS. Though the chromosomal location varies, we can see that these TssI2 C-terminal homologs exist as C-terminal extensions of evolved VgrGs among these species. Interestingly, solitary TssI2 C-terminal-TsiI2 modules, independent of VgrG, are also present which are mainly found in *V. alginolyticus, Aeromonas salmonicida*, and *Marinomonas primoryensis*. Especially, the orphan TssI2 C-terminal-TsiI2 modules in *M. primoryensis* are commonly associated with transposase alone or together with integrase, indicating that this genetic module could be horizontally transferred among microbes within the same niche.

Investigating the key residues in TssI2 C-terminal

Our bioinformatics analysis predicted the existence of the Pst domain in the TssI2 C-terminal region. The structural architecture and functional mechanism of Pst from *Y. pestis* have been revealed, which is composed of a translocation (Pst^T, residues 1–40), a receptor binding (Pst^R, residues 41–166), and an activity domain (Pst^A, residues 167–357)[52] (Figure 4a). The crystal structure of Pst (PDB code 4AQN) reveals a phage T4 lysozyme fold of the activity domain, which determines the protein's lethal activity.[52] To further characterize the active center of the TssI2 C-terminal region, we employed sequence comparison, structural modeling, and mutagenic analysis. The sequence alignment between TssI2 and *Y. pestis*'s Pst showed that residues 858–1010 of TssI2 had 33% amino acid identity to the Pst^A (residues 196–349) (Figure 4a). Then we compared the key features in protein structures between TssI2 C-terminal (residues 834–1012) and Pst^A with ENDscript server and PyMol software, and our results showed high conservation in the primary sequence and overall folding structure (Figure 4b and 4c).[52] Especially, the residues within and around Pst's small β-strands β8, β10, β11, as well as α5 helix display much higher conservation than residues at other positions. Based on the structural alignment of TssI2 C-terminal and Pst^A, combined with reported key residues in Pst, we selected five equivalent residues in TssI2 to verify their functional contribution to the toxicity of the TssI2 C-terminal. Specifically, Glu-844, Pro-853, Thr-863, Asp-869, and Gln-963 of TssI2 were selected for alanine substitutions, and the 834–1012 segment without Sec signal peptide was used as a negative control since TssI2 C-terminal exerted toxic effect only when located in periplasmic space
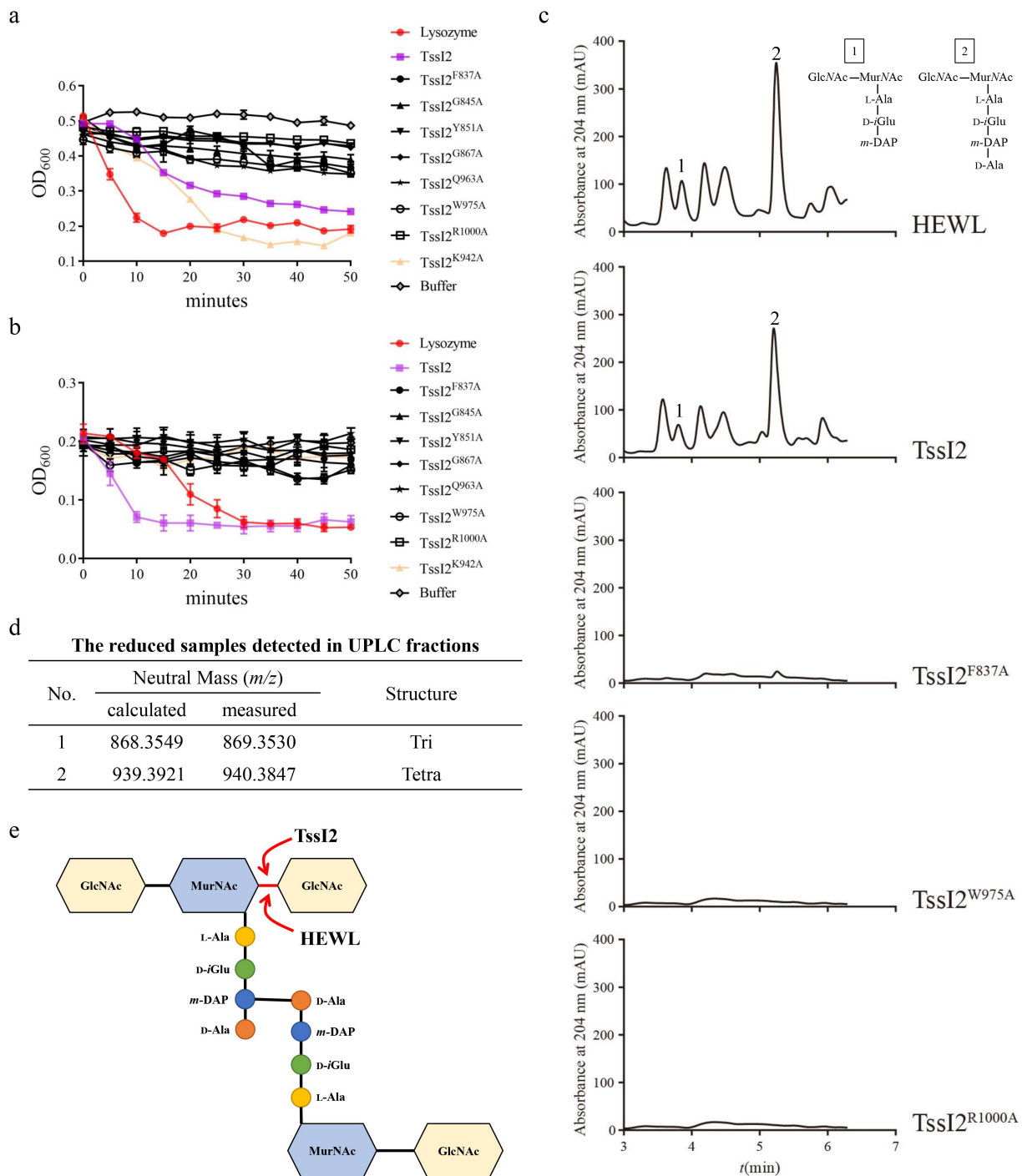
Figure 5. Confirmation of the contribution of selected conserved residues to TssI2 activity and determination of the PG hydrolysis products of TssI2 by UPLC-MS analysis. (a) (b) Incubation of recombinant TssI2 (purple), TssI2^{K942A} (orange), other variants (black) and HEWL (red) with polymyxin B-permeabilized *E. coli* cells (a) or purified PG (b). A decrease in turbidity indicates bacterial lysis or PG hydrolysis. HEWL acts as a positive control, while the buffer-only condition acts as the negative control. Points and error bars represent the mean ± SEM (n = 3 biological replicates). (c) UPLC chromatograms of PG hydrolysis products by recombinant TssI2 and its variants. The purified PG was digested by HEWL, recombinant TssI2, TssI2^{F837A}, TssI2^{W975A}, or TssI2^{R1000A}, and reduced by sodium borohydride, then filtered by 0.22 μm filter membrane (Millex, SLGV004SL). The flow-through samples were collected for UPLC analysis. The fractions of peak 1 and 2 were then identified by mass spectrometry (see also Figure S5), and structures of the muropeptides are shown. Abbreviations: GlcNAc, N-acetylglucosamine; MurNAc, N-acetylmuramic acid; L-Ala, L-alanine; D-*i*Glu, D-*iso*glutamic acid; *m*DAP, *meso*-diaminopimelic acid; D-Ala, D-alanine. (d) Neutral masses of fractions of peak 1 and 2 from UPLC. (e) Simplified representation of the inferred TssI2 cleavage site on a PG dimer based on data summarized in (b) to (d). Abbreviations are the same as in (c).

of bacteria. These mutant derivatives were cloned into pSRKGm with an N-terminal Sec-tag and a C-terminal His-tag and their bactericidal activities were tested in *E. coli* MG1655. TssI2$^{834-1012}$$^{(E844A)}$, TssI2$^{834-1012(T863A)}$, TssI2$^{834-1012(D869A)}$, and TssI2$^{834-1012(Q963A)}$ exhibited no toxicity, while TssI2$^{834-1012(P853A)}$ showed a slight loss of toxicity (Figure 4d). The loss of function was not due to the defects of protein expression as Western blot analysis showed that all TssI2 mutants were well expressed (Figure S3). The mutation effects of Glu-844, Thr-863, Asp-869 in TssI2 are consistent with those of Glu-178, Thr-201, and Asp-207 in Pst from *Y. pestis* where these three residues were identified as active sites.[52] The major difference was found between Gln-963 of TssI2 and Gln-301 of Pst. Mutation of Gln-963 resulted in complete loss of bactericidal activity of TssI2 C-terminal, while alanine substitution of Gln-301 in Pst barely led to about 20% reduction of the enzymatic activity as estimated by the diameters of pesticin lysis zones.[52]

Alphafold2 analysis revealed that TssI2 C-terminal is composed of nine α-helicals and four small β-strands and could roughly be divided into two components, namely the TssI2 C-terminal domain 1 (TssI2^{CD1}, residue 834–928) and 2 (TssI2^{CD2}, residue 929–1012), which are connected by the long α-helical segment α5. The predicted structure of TssI2 C-terminal matched closely to Pst^A with a root mean square deviation (RMSD) value of 1.96 Å between each other. We also identified the surface cavity using CASTp 3.0 software,[53] and recognized a clear pocket between the TssI2^{CD1} and TssI2^{CD2} (Figure 4e), indicating a potential active center. This prediction was supported by the alanine substitution analysis of three residues (Glu-844, Thr-863, and Asp-869) in the pocket, which resulted in the loss of bactericidal activity (Figure 4d).

To identify other potential key residues in TssI2 C-terminal, we performed multiple alignments of 473 TssI2 C-terminal homolog proteins previously retrieved from the non-redundant database of NCBI based on Pst^A domain search. Sequence alignments revealed additional highly conserved residues except for the above-mentioned five ones (Figure 4f). As a result, we selected additional seven residues for alanine substitutions to examine their

contributions to TssI2 C-terminal bactericidal activity. Gly-845, Gly-867, Tyr-851, and Arg-1000 of TssI2 were chosen due to their proximity to the surface cavity (Figure 4e and 4f). Another two strictly conserved residues, Phe-837 and Trp-975, were also selected, despite being distant from the cavity (Figure 4e and 4f). Lys-942 was selected as a possible negative control because of its low conservation. As shown in Figure 4g, TssI2$^{834-1012}$$^{(G845A)}$, TssI2$^{834-1012(Y851A)}$, TssI2$^{834-1012(G867A)}$, TssI2$^{834-1012(F837A)}$, TssI2$^{834-1012(W975A)}$, and TssI2$^{834-1012(R1000A)}$ all lost bactericidal activities when expressed in the periplasmic space of MG1655 though Western blotting showed they were all highly expressed, while TssI2$^{834-1012}$$^{(K942A)}$ maintained toxicity (Figure 4g and S4). However, our effects to purify the TssI2$^{834-1012}$ and its variant proteins failed due to the formation of inclusion bodies under tested experimental conditions.

To further clarify the role of the conserved residues to TssI2 activity, we selected Gln-963, which displayed a different mutation phenotype from the counterpart Gln-301 of *Y. pestis* Pst, and above seven newly-identified ones as representatives and constructed recombinant expression plasmids pET30a-TssI2^{F837A}, pET30a-TssI2^{G845A}, pET30a-TssI2^{Y851A}, pET30a-TssI2^{G867A}, pET30a-TssI2^{K942A}, pET30a-TssI2^{Q963A}, pET30a-TssI2^{W975A}, and pET30a-TssI2^{R1000A} for soluble TssI2 variant proteins expression and purification. We employed an outside-in approach, where the purified proteins were incubated with polymyxin B-permeabilized MG1655 with an initial cell density of 0.5 at OD$_{600}$ and the culture turbidity was monitored at five-minute intervals for 50 minutes. Hen egg-white lysozyme (HEWL) and wild-type TssI2 were used as positive controls, while buffer alone served as a negative control. As shown (Figure 5a), the wild-type TssI2 and TssI2^{K942A} variants both caused obvious drop of OD$_{600}$ of the culture as HEWL, while the TssI2 variants TssI2^{F837A}, TssI2^{G845A}, TssI2^{Y851A}, TssI2^{G867A}, TssI2^{Q963A}, TssI2^{W975A}, and TssI2^{R1000A} lost the ability to kill MG1655 similar to the corresponding C-terminal TssI2$^{834-1012}$ variants containing the same specific residue substitutions
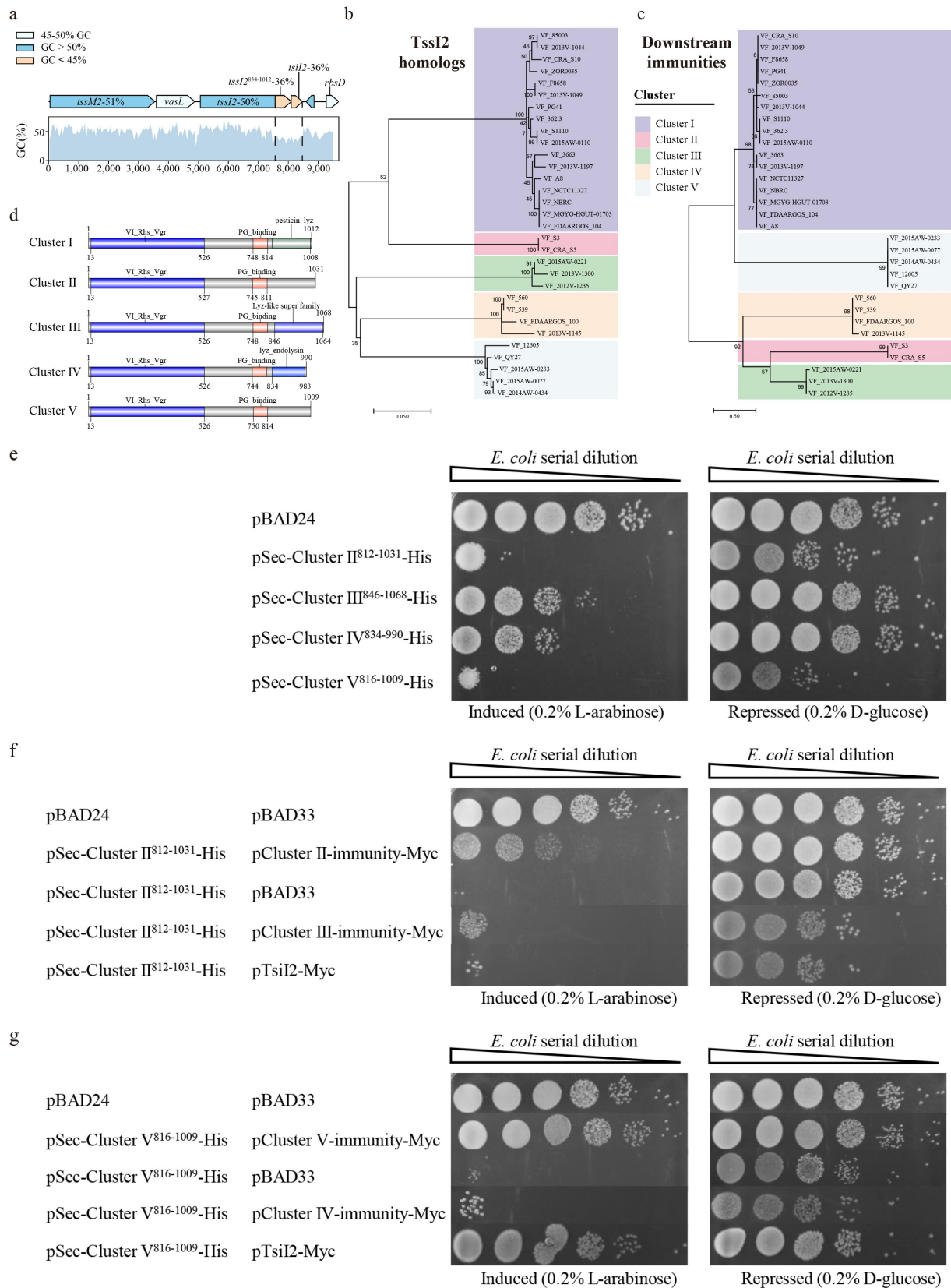
Figure 6. Conservation analyses of TssI2 in *V. fluvialis*. (a) Sliding window analyses of GC content of VflT6SS2 region from *tssM2* to *rbsD* in *V. fluvialis* 85003. The Y axis is the GC%, and the X axis indicates the relative distance (bp) from the start of the *tssM2* gene. The size of the sliding window was 50 bp. (b) (c) Phylogenetic trees of VflT6SS2 TssI2-TsiI2 modules in various *V. fluvialis* strains. Phylogenetic trees were constructed using maximum likelihood methods with the Whelan And Goldman + Freq. model based on homology of TssI2 (b) or

(Figure 4d and 4g). These results proved again that the conserved residues Phe-837, Gly-845, Tyr-851, Gly-867, Gln-963, Trp-975, and Arg-1000 are also critical for the bactericidal activity of TssI2. To provide additional *in vitro* evidence of PG hydrolysis activity of TssI2 and its variants, we incubated the proteins with purified MG1655 PG and measured the turbidity at OD_{600} during the incubation. Consistently, HEWL and wild-type TssI2 instead of variants resulted in a rapid drop in the turbidity of the suspension indicating that the PG material is hydrolyzed (Figure 5b). Out of expectation, $TssI2^{K942A}$ variant displayed no hydrolysis activity on PG. We reasoned that this may be due to less optimal hydrolysis condition *in vitro* than *in vivo* for $TssI2^{K942A}$. Together, these results demonstrated that except Glu-844, Thr-863, and Asp-869, which constitute the originally proposed Glu-Asp-Thr catalytic triad, other highly conserved residues are also required for the bactericidal function or enzymatic activity of TssI2. We deduced that these residues probably play a necessary role in assisting folding or stabilization of the active site of the enzyme or participating in substrate binding.

Subsequently, we identified the soluble PG hydrolysis products of TssI2 by ultra-performance liquid chromatography (UPLC)-tandem mass spectrometry (MS) analysis. The LC separation profile of TssI2-digested PG is highly similar to that of HEWL, indicating that TssI2 cleaves the β-1,4-glycosidic bond between *N*-acetylmuramic acid (MurNAc) and *N*-acetylglucosamine (GlcNAc) residues of PG (Figure 5c and 5e). While the variant representatives $TssI2^{F837A}$, $TssI2^{W975A}$, and $TssI2^{R1000A}$ displayed significantly diminished activity, no soluble peptidoglycan fragments were released (Figure 5c). The molecular masses as well as

MS spectra (Figure 5d and S5) support peak assignments for the muramidase/lysozyme products. The peaks at *m/z* 869 and 940, respectively, correspond to GlcNAc–MurNAc–L-Ala–D-*i*Glu–*m*DAP (Tri) and GlcNAc–MurNAc–L-Ala–D-*i*Glu–*m*DAP–D-Ala (Tetra) which is the major component of *E. coli* cell wall.

Conservation analysis of evolved VgrG of VflT6SS2 in *V. fluvialis* isolates

Sliding-window analysis of GC content of the VflT6SS2 major gene cluster revealed extremely low GC content of *tssI2* C-terminal and *tsiI2* compared to their surrounding sequences (Figure 6a). Both *tssI2* C-terminal (2500–3039 bp) and *tsiI2* have GC contents of 36%, while their flanking sequence reaches around 50%. The unique composition and mode structure denote a possibility of horizontal acquisition of the *tssI2* C-terminal and its following *tsiI2* gene. So, we speculated that the *tssI2-tsiI2* genetic modules of VflT6SS2 might have much sequence variation in different *V. fluvialis* isolates.

To test this presumption, we searched the proteins of the VflT6SS2 cluster using BLASTp analysis against 31 *V. fluvialis* strains of the GenBank database (Supplementary Data 3) and compared the protein sequences of TssI2-TsiI2 effector-immunity modules. The phylogenetic classification of TssI2 homologs (Figure 6b) or their downstream immunities (Figure 6c) revealed five clusters for these effector-immunity loci. Each cluster corresponds to a conserved TssI2-TsiI2 module. Cluster I seems to be the most popular one and makes up 55% of the analyzed TssI2-TsiI2 homologs, including the module studied here. The compositions of the five clusters were conserved by, respectively, comparing TssI2 and TsiI2 phylogenetic trees, i.e., there are good corresponding relations between the effector and immunity. However,

downstream immunity (c) from 31 *V. fluvialis* isolates. Strain names were used to indicate the corresponding effectors or cognate immunity proteins, and the same color marked the same cluster between Figure 6b and 6c. (d) Schematic representation of the domain architectures of VgrG effectors representing five different clusters. (e) Survival of *E. coli* expressing C-terminal regions of representative effectors from Clusters II to V. The proteins are targeted to the periplasm by the Sec-tag. 10-fold serial dilutions of cultures were spotted on LB agar containing inducer or repressor at the indicated concentrations and were grown overnight at 37℃. (f) (g) Growth of *E. coli* expressing C-terminal region of the Cluster II or V effector alone, or co-expressing effector and its cognate immunity or non-cognate immunity, such as Cluster III, IV, or TsiI2 immunity, under inducing or repressing condition.

the phylogenetic relationships of the five clusters between the two trees were inconsistent, indicating the possibility of recombination during the TssI2-TsiI2 module evolution. To simplify the analysis, we selected an effector protein from each cluster as a representative and performed multiple sequence alignments of these five TssI2 homologous proteins. The results showed that the N-terminals of these representative sequences share 95%–98% identity, but their C-terminals exhibit very low identity (12%–22%) (Figure S6). Conserved domain analysis using Pfam service showed that the C-terminals of Cluster III (residues 846–1064) and IV (residues 834–983) proteins belong to the lysozyme family, whereas the C-terminals of Cluster I homologs harbor the Pst[A] domain. Nevertheless, no known domains were predicted in the C-terminals of Cluster II and V (Figure 6d). Beyond our expectation, the representative protein sequence of Cluster II shares 68% identity and 100% coverage with *V. cholerae* VgrG3 (VCA0123), which has a hydrolase activity and degrades PG in the periplasm of target bacteria.[54] The overall structure of the C-terminal of VgrG3 owns a T4-lysozyme-like architecture.[32] Therefore, we intended to test whether the highly variable C-terminal of the representative proteins of Cluster II to V conferred the antibacterial activity as TssI2. For this purpose, we cloned the C-terminus of the representative proteins with an N-terminal Sec-tag and a C-terminal His-tag into the pBAD24 vector, which can be induced by L-arabinose or repressed by D-glucose. As shown in Figure 6e, induction of pSec-Cluster II$^{812-1031}$-His, pSec-Cluster III$^{846-1068}$-His, pSec-Cluster IV$^{834-990}$-His, and pSec-Cluster V$^{816-1009}$-His greatly inhibited the growth of host *E. coli* BL21 (DE3) compared to the empty vector. Notably, the pSec-Cluster II$^{812-1031}$-His and pSec-Cluster V$^{816-1009}$-His exhibited the strongest bactericidal activity with >10^4-fold inhibitory effect under induced conditions and even showed substantial killing activity under glucose-repressed conditions.

Then, Cluster II$^{812-1031}$ and Cluster V$^{816-1009}$, the two C-terminus proteins with the highest bactericidal activity, were selected to investigate whether their downstream adjacent gene products could provide immunity protection. We introduced the coding genes of the downstream proteins of Cluster II and Cluster V representative effectors into the pBAD33 vector and co-expressed with their respective C-terminal effector constructs in *E. coli* BL21(DE3). For convenient monitoring of the putative immunity expression, a Myc-tag was added to the C-terminus of the proteins. The co-expression experiments showed that both Cluster II and V immunities provided substantial protection against the toxicities of their corresponding effectors compared to the empty vector control (Figure 6f and 6g). The protection efficiency of Cluster V immunity to its effector seems higher than that of Cluster II. We also tested the cross-protection of non-cognate immunity to Cluster II and Cluster V effectors. The results showed that the Cluster III immunity and TsiI2 (belongs to Cluster I) could not efficiently refrain from the toxicity of the Cluster II effector (Figure 6f). However, the toxicity of Cluster V effector was significantly inhibited by TsiI2, but not by Cluster IV immunity (Figure 6g). These results revealed that the evolved VgrG effectors and cognate immunities in the *V. fluvialis* VflT6SS2 homologous locus were genetically diverse. The immunity protected host bacteria from being killed by the cognate effector. Of note, certain immunity could provide cross-protection against its non-cognate VgrG effector.

Discussion

In this study, we analyzed and characterized TssI2-TsiI2, a new effector-immunity pair in the VflT6SS2 of *V. fluvialis* and demonstrated that TssI2 is toxic when located in target cell periplasm by employing its lysozyme activity. TsiI2, which is located downstream and adjacent to TssI2, interacts with and antagonizes the antibacterial activity of TssI2. As we know, many T6SS effectors targeting cell walls[22,23,28,32,55–57] were classified as cargo effectors, except VgrG3 in *V. cholerae* and VgrG2b in *P. aeruginosa*, which belong to evolved VgrG or specialized effectors.[1] Here, we provided evidence to support that the TssI2 in *V. fluvialis* VflT6SS2 is a new member of the specialized VgrG effector family.

Pst is a key bacteriocin secreted by *Y. pestis* and some pathogenic *E. coli* strains to kill associated bacteria of the same niche.[47,52] Our current study

discovered that the C-terminal of TssI2 is highly homologous to the Pst[A] domain of *Y. pestis* Pst toxin and seems to be fully responsible for the killing activity of TssI2. To our knowledge, this is for the first time we identified a T6SS effector containing an active Pst[A] domain, and disclosed a broad distribution of this domain in various forms in Proteobacteria, especially with high prevalence in γ-Proteobacteria. These results indicate that the Pst[A] domain can be integrated with many other functional domains and may participate in various biological processes of host cells. Especially, the adoption of the Pst[A] domain as an effective antibacterial weapon by T6SS greatly broadened the biological killing targets of this active domain compared with the Pst toxin itself, whose targets are strictly narrowed to those carrying the FyuA receptor responsible for the Pst uptake.[52] The distribution diversity of the Pst[A] domain also suggests that its integration may be related to horizontal gene transfer.

Pst is unique among the bacteriocins in that it targets the periplasmic PG. Although, we proved that TssI2 C-terminal also executes its functions in periplasm, the spatial structure and conserved residues of the TssI2 C-terminal are not completely identical to those of the Pst[A] domain. Supporting this assumption, TssI2 was identified to be able to hydrolyze fluorescence-labeled *M. lysodeikticus* cell walls and purified *E. coli* PG *in vitro* (Figure 2d and 5b), while Pst failed to do so.[52] Additionally, the mutant of Gln-963 of TssI2 almost completely lost its ability to inhibit host bacterial growth while that of the equivalent Gln-301 of Pst demonstrated only about 20% reduction of the enzymatic activity.[52] By using UPLC-MS analysis, we further confirmed that TssI2 hydrolyzes the β-1,4-glycosidic bond between MurNAc and GlcNAc residues of PG substrate (Figure 5c to 5e).

In pesticin, Pst[AD1] and Pst[AD2] form a pocket with an approximate diameter of 1 nm, which is for substrate binding.[52] TssI2[CD1] and TssI2[CD2] were predicted to form a similar pocket (Figure 4e). Based on sequence alignments of several hundreds of Pst[A] domain-containing proteins, more strictly conserved residues surrounding the TssI2 substrate-binding pocket were proved to be essential to the killing activity of TssI2 in periplasmic space (Figure 4e to 4g and Figure 5a). Among

the residues, two of them are even located far away from the pocket (Figure 4e). Therefore, our current work uncovered more previously unrecognized conserved residues inside and outside the putative active pocket that is required for the bactericidal activity of TssI2. These residues probably participate in substrate-specific binding and maintenance of proper conformation of the domain. Yet, the exact roles of these residues remain to be further defined.

There are a total of four VflT6SS2 VgrGs in *V. fluvialis* 85003. TssI2 at the VflT6SS2 major cluster is the only specialized VgrG effector. The other three homologs, TssI2_a, TssI2_b, and TssI2_c, located at three orphan clusters, do not have any C-terminal extensions.[42] T6SS-wielding bacteria typically employ diverse effectors for the interbacterial competition, which are species-specific or even strain-specific. Cognate immunities are usually located downstream and adjacent to the effector genes and protect their host from neighboring bacterial effector attacks. In this study, we confirmed that TssI2-TsiI2 is a genuine effector-immunity pair from the locus, physical interaction, functional antagonism, and cellular co-localization. The *V. fluvialis* TssI2-TsiI2 module search revealed that this specific effector-immunity pair also exists in several pathogenic *Vibrio* species, such as *V. anguillarum, V. cholerae*, and *V. alginolyticus*, etc., implying that these species could coexist in the same niche.

Based on the sequence homologies of TssI2-TsiI2 modules in different *V. fluvialis* isolates, TssI2 C-terminal extension and TsiI2 were individually classified into five clusters. Despite the relatively low protein sequence identity (14%–22%) among the Clusters, each representative of the C-terminal extension selected was proved to have bactericidal activity with vastly varying degrees. To be specific, Cluster II and V displayed more potent killing effects than Cluster III and IV, despite no apparent domain being predicted from the former two. In addition, cross-protection was identified in this study since TsiI2 immunity from Cluster I provided full protection against Cluster V effector. Two possible explanations exist, and one is due to the similar spatial conformation between effectors of Cluster V and I though they share only 15% sequence identity, and the other

may come from the immunity side, i.e. TsiI2 probably mimic Cluster V immunity, and this deduction is somehow supported by the fact that they share 27% identity that is the highest among the five types of cluster immunities. However, it is worth noting that though Cluster III immunity has as high as 22% identity with Cluster V immunity, no cross-protection was observed. Generally, the relationship between the toxic effector and its cognate immunity is specific. The organization of toxic effector-immunity pairs enables them to be easily fused to various effector classes.[58] The cross-protection of immunity to a non-cognate effector is rare. However, increasing evidence shows that bacteria may retain or actively accumulate "orphan" immunities for effectors, which they do not have, adopting as a strategy to protect themselves against T6SS attacks from other bacteria.[59] The cross-protection works simply through acquiring bi- or multi-functional immunity proteins and therefore is a more cost-effective approach.

The modular genetic architecture and drastic GC content variation of the composition sequences of *tssI2-tsiI2* in *V. fluvialis* VflT6SS2 suggest a possible exchange and horizontal acquisition of this toxin-immunity pairs.[60] It is also possible that exogenous toxin domains evolve independently, as closely related strains contain dramatic sequence variations. These different mechanisms greatly increase the diversity of toxic cargos.[58] Through repeat sequence search, we tried to identify the potential integration or exchange site of the VflT6SS2 major cluster C-terminal toxin-immunity pairs on the chromosome but failed to get a potential candidate sequence. Unexpectedly, we found that strain CRA_S5 whose VgrG effector belongs to Cluster II carries an identical copy of the immunity gene of Cluster III effector and strain FDAARGOS_100, which is sub-grouped into Cluster IV carries a duplicate copy of the immunity gene of Cluster V effector (Figure S7). These data suggest that the heterologous exchange or transfer of the C-terminal of evolved VgrG and its immunity occurs, and the existence of multiple copies of immunity proteins may help to enhance interspecies and intraspecies antibacterial competitiveness

in their niche. However, the origin of the five clusters of evolved VgrG effectors and their cognate immunities and the mechanism that effectors and immunities horizontally transfer still needs to be further explored.

In conclusion, our current work identified a new evolved VgrG effector TssI2 and its immunity TsiI2 from VflT6SS2 in *V. fluvialis*, and characterized their sequences, structures, functions, possible evolution mechanism, and biological relevance. These findings will aid us to get a better understanding of the bacterial type VI secretion system and its functions in mediating interspecies and intraspecies antibacterial competitiveness.

Materials and Methods

Strains and media

The bacterial strains and plasmids used in this study were listed in Table 1 VF85003 and its derivatives were routinely grown in Luria-Bertani (LB) broth (pH 7.4) containing 170 mM NaCl at 30°C unless specifically indicated. *E. coli* strain DH5αλpir, SM10λpir, MG1655, BL21(DE3), XL1-Blue and BTH101 were routinely cultured at 37°C. Culture media were supplemented with ampicillin (Amp, 100 μg/ml), streptomycin (Sm, 100 μg/ml), rifampicin (Rfp, 50 μg/ml), kanamycin (Km, 50 μg/ml), tetracycline (Tc, 10 μg/ml for *E. coli*, 2.5 μg/ml for *V. fluvialis*), chloramphenicol (Cm, 10 μg/ml), gentamicin (Gm, 50 μg/ml), L-arabinose, D-glucose, or isopropyl-β-D-thiogalactopyranoside (IPTG), if required.

Plasmid construction

For IPTG-inducible expression in bacteria, DNA fragments corresponding to the full-length or truncated forms of *tssI2* or *tsiI2* were amplified from *V. fluvialis* 85003 genomic DNA. PCR fragments were inserted into the multiple cloning sites (MCS) of the pSRKGm vector harboring a gentamicin-resistance cassette, pSRKTc vector with a tetracycline-resistance one or pMALc2x vector with an ampicillin-resistance gene.

Table 1. Bacterial strains and plasmids used in this study.

Strains/Plasmids	Characteristics	Reference/Source
E. coli		
DH5α*pir*	F-D(*lacZYA-argF*)U169*recA endA1 supE44 relA1*λ::*pir*	Laboratory stock
SM10λ*pir*	*thr thi tonA leu supE lacY recA*::RP4-2Tc::Mu (λ*pir*R6 K), Km[R]	Laboratory stock
MG1655	K-12 F⁻ λ⁻ *ilvG⁻ rfb-50 rph-1*, Rfp[R]	Laboratory stock
BL21(DE3)	F⁻ *ompT hsdS* (rB⁻ mB⁻) *gal dcm* (DE3)	Laboratory stock
BL21(DE3)pLysS	F- *ompT hsdS* (rB⁻ mB⁻) *gal dcm* (DE3) pLysS, Cm[R]	Laboratory stock
XL1-Blue	*endA1 gyrA96*(*nal*[R]) *thi-1 recA1 relA1 lac glnV44* F′[::Tn10 *proAB*⁺ *lacI*[q] Δ(*lacZ*)M15] *hsdR17*(rK⁻ mK⁺)	Laboratory stock
BTH101	F⁻ *cya-99 araD139 galE15 galK16 rpsL hsdR mcrA1 mcrB1*	Laboratory stock
V. fluvialis		
WT	*V. fluvialis* 85003, wild type, Sm[R]	Laboratory stock
Δ*vasK*	85003 with *vasK* in-frame deletion, Sm[R]	Laboratory stock
Δ*vasH*	85003 with *vasH* in-frame deletion, Sm[R]	[42]
Δ*tssI2*	85003 with *tssI2* in-frame deletion, Sm[R]	This study
Δ*tssI2-tsiI2*	85003 with *tssI2* and *tsiI2* in-frame deletion, Sm[R] (attacker) or Rif[R] (prey)	This study
Pathogenic *Vibrios*		
V. cholerae A1552	toxigenic wild type *V. cholerae*, O1 El Tor Inaba (Latin America isolate, 1992)	[61]
V. cholerae C7258	toxigenic wild type *V. cholerae* O1 El Tor Ogawa (Peru isolate, 1991)	[62]
V. cholerae 93097	nontoxigenic wild type *V. cholerae*, O1 El Tor Ogawa	Laboratory stock
V. alginolyticus ATCC17749	*V. alginolyticus* reference strain	Laboratory stock
V. vulnificus ABH2018-w-021	wild type *V. Vulnificus*, biotype 3	Laboratory stock
Plasmids		
pWM91	Suicide vector containing R6 K *ori*, *sacB*, *lacZa*; Amp[R]	Laboratory stock
pSRKTc	Broad-host-range vector containing *lac* promoter, *lacI*[q], *lacZa*⁺, Tet[R]	Laboratory stock
pTsiI2	TsiI2 cloned at *NdeI*/*XbaI* sites in pSRKTc	This study
pTssI2	TssI2 cloned at *NdeI*/*XhoI* sites in pSRKTc	This study
pMALc2x	Cloning vector with *lac* promoter, *lacI*[q], Amp[R]	Laboratory stock
pMAL-TsiI2-Myc	TsiI2 with a C-terminal Myc-tag in pMALc2x	This study
pSRKGm	Broad-host-range vector containing lac promoter and *lacI*[q], *lacZa*⁺, Gm[R]	Laboratory stock
pTssI2-His	TssI2 with a C-terminal His-tag in pSRKGm	This study
pSec-TssI2¹⁻⁸³³-His	TssI2[1-833] with an N-terminal Sec-secretion signal and a C-terminal His-tag in pSRKGm	This study
pSec-TssI2⁷⁴⁷⁻⁹⁸⁴-His	TssI2[747-984] with an N-terminal Sec-secretion signal and a C-terminal His-tag in pSRKGm	This study
pSec-TssI2⁸³⁴⁻⁹⁸⁴-His	TssI2[834-984] with an N-terminal Sec-secretion signal and a C-terminal His-tag in pSRKGm	This study
pSec-TssI2⁸³⁴⁻¹⁰¹²-His	TssI2[834-1012] with an N-terminal Sec-secretion signal and a C-terminal His-tag in pSRKGm	This study
pSec-TssI2⁹²⁷⁻¹⁰¹²-His	TssI2[927-1012] with an N-terminal Sec-secretion signal and a C-terminal His-tag in pSRKGm	This study
pET30a(+)	Expression vector containing f1 *ori*, *lacI*; Kan[R]	Laboratory stock
pET30a-TssI2	TssI2 cloned at *NdeI*/*XhoI* sites in pET30a(+)	This study
pET30a-TsiI2¹⁹⁻¹²⁷	TsiI2[19-127] cloned at *NdeI*/*XhoI* sites in pET30a(+)	This study
pKT25	BACTH vector with T25 fragment of CyaA (amino acids 1–224); *plac*, p15A *ori*, Km[R]	Laboratory stock
pUT18C/pUT18	BACTH vector with T18 fragment of CyaA (amino acids 225–339); *plac*, ColE1 *ori*, Amp[R]	Laboratory stock
pKT25-zip	Leucine zipper of yeast protein GCN4 fused in frame with T25 in pKT25	Laboratory stock
pUT18C-zip	Leucine zipper of yeast protein GCN4 fused in frame with T18 in pUT18C	Laboratory stock
pT25-TssI2	TssI2 fused at C-termini of T25 in pKT25	This study
pT18-TsiI2¹⁹⁻¹²⁷	TsiI2[19-127] fused at C-termini of T18 in pUT18C	This study
pTsiI2¹⁹⁻¹²⁷-T18	TsiI2[19-127] fused at N-termini of T18 in pUT18	This study
pT25-TsiI2¹⁹⁻¹²⁷	TsiI2[19-127] fused at C-termini of T25 in pKT25	This study
pTssI2⁸³⁴⁻¹⁰¹²-His	TssI2[834-1012] with a C-terminal His-tag in pSRKGm	This study
pVgrG3⁷²⁷⁻¹⁰¹⁷-His	*V. cholerae* N16961 VgrG3[727-1017] with a C-terminal His-tag in pSRKGm	This study
pTsiI2¹⁹⁻¹²⁷-Myc	TsiI2[19-127] with a C-terminal Myc-tag in pBAD24	This study
pBAD24	Cloning vector with pBAD promoter, ColE1 *ori*, *araC*, Amp[R]	Laboratory stock
pSec-TssI2⁸³⁴⁻¹⁰¹²(E844A)-His	E844A mutant of TssI2[834-1012] with an N-terminal Sec-secretion signal and a C-terminal His tag in pSRKGm	This study
pSec-TssI2⁸³⁴⁻¹⁰¹²(P853A)-His	P853A mutant of TssI2[834-1012] with an N-terminal Sec-secretion signal and a C-terminal His-tag in pSRKGm	This study
pSec-TssI2⁸³⁴⁻¹⁰¹²(T863A)-His	T863A mutant of TssI2[834-1012] with an N-terminal Sec-secretion signal and a C-terminal His-tag in pSRKGm	This study
pSec-TssI2⁸³⁴⁻¹⁰¹²(D869A)-His	D869A mutant of TssI2[834-1012] with an N-terminal Sec-secretion signal and a C-terminal His-tag in pSRKGm	This study
pSec-TssI2⁸³⁴⁻¹⁰¹²(Q963A)-His	Q963A mutant of TssI2[834-1012] with an N-terminal Sec-secretion signal and a C-terminal His-tag in pSRKGm	This study
pSec-TssI2⁸³⁴⁻¹⁰¹²(F837A)-His	F837A mutant of TssI2[834-1012] with an N-terminal Sec-secretion signal and a C-terminal His-tag in pSRKGm	This study
pSec-TssI2⁸³⁴⁻¹⁰¹²(G845A)-His	G845A mutant of TssI2[834-1012] with an N-terminal Sec-secretion signal and a C-terminal His-tag in pSRKGm	This study

(Continued)

Table 1. (Continued).

Strains/Plasmids	Characteristics	Reference/Source
pSec-TssI2$^{834-1012(Y851A)}$-His	Y851A mutant of TssI2$^{834-1012}$ with an N-terminal Sec-secretion signal and a C-terminal His-tag in pSRKGm	This study
pSec-TssI2$^{834-1012(G867A)}$-His	G867A mutant of TssI2$^{834-1012}$ with an N-terminal Sec-secretion signal and a C-terminal His-tag in pSRKGm	This study
pSec-TssI2$^{834-1012(W975A)}$-His	W975A mutant of TssI2$^{834-1012}$ with an N-terminal Sec-secretion signal and a C-terminal His-tag in pSRKGm	This study
pSec-TssI2$^{834-1012(R1000A)}$_His	R1000A mutant of TssI2$^{834-1012}$ with an N-terminal Sec-secretion signal and a C-terminal His-tag in pSRKGm	This study
pSec-TssI2$^{834-1012(K942A)}$-His	K942A mutant of TssI2$^{834-1012}$ with an N-terminal Sec-secretion signal and a C-terminal His-tag in pSRKGm	This study
pET30a-TssI2^{Q963A}	Q963A mutant of TssI2 cloned at *Nde*I/*Xho*I sites in pET30a(+)	This study
pET30a-TssI2^{F837A}	F837A mutant of TssI2 cloned at *Nde*I/*Xho*I sites in pET30a(+)	This study
pET30a-TssI2^{G845A}	G845A mutant of TssI2 cloned at *Nde*I/*Xho*I sites in pET30a(+)	This study
pET30a-TssI2^{Y851A}	Y851A mutant of TssI2 cloned at *Nde*I/*Xho*I sites in pET30a(+)	This study
pET30a-TssI2^{G867A}	G867A mutant of TssI2 cloned at *Nde*I/*Xho*I sites in pET30a(+)	This study
pET30a-TssI2^{W975A}	W975A mutant of TssI2 cloned at *Nde*I/*Xho*I sites in pET30a(+)	This study
pET30a-TssI2^{R1000A}	R1000A mutant of TssI2 cloned at *Nde*I/*Xho*I sites in pET30a(+)	This study
pET30a-TssI2^{K942A}	K942A mutant of TssI2 cloned at *Nde*I/*Xho*I sites in pET30a(+)	This study
pSec-Cluster II$^{812-1031}$-His	DM587_R00760$^{812-1031}$ with a C-terminal His-tag in pBAD24	This study
pSec-Cluster III$^{846-1068}$-His	GPY10_RS21745$^{846-1068}$ with a C-terminal His-tag in pBAD24	This study
pSec-Cluster IV$^{834-990}$-His	AL475_RS00350$^{834-990}$ with a C-terminal His-tag in pBAD24	This study
pSec-Cluster V$^{816-1009}$-His	BV404_RS19285$^{816-1009}$ with a C-terminal His-tag in pBAD24	This study
pBAD33	Cloning vector with pBAD promoter, p15A *ori, araC*, Cm^R	Laboratory stock
pCluster II-immunity-Myc	DM587_00765 with a C-terminal Myc-tag in pBAD33	This study
pCluster III-immunity-Myc	GPY10_RS21750 with a C-terminal Myc-tag in pBAD33	This study
pCluster IV-immunity-Myc	AL475_RS00345 with a C-terminal Myc-tag in pBAD33	This study
pCluster V-immunity-Myc	BV404_RS19280 with a C-terminal Myc-tag in pBAD33	This study
pTsiI2-Myc	TsiI2 with a C-terminal Myc-tag in pBAD33	This study

To check the toxicity of the representative effectors, the C-terminals of *V. fluvialis* CRA_S5 DM587_RS00760 (Cluster II$^{812-1031}$), *V. fluvialis* 2013 V-1300 GPY10_RS21745 (Cluster III$^{846-1068}$), *V. fluvialis* FDAARGOS_100 AL475_RS00350 (Cluster IV$^{834-990}$), and *V. fluvialis* 12605 BV404_RS19285 (Cluster V$^{816-1009}$) were synthesized at Tsingke Biological Technology and cloned into pBAD24 vector. To test the protection of immunity against effector, TsiI2 (Cluster I), DM587_RS00765 (Cluster II), PY10_RS21750 (Cluster III), AL475_RS00345 (Cluster IV), and BV404_RS19280 (Cluster V) was synthesized and cloned into pBAD33. All constructs were confirmed by DNA sequencing and listed in Table 1.

Construction of mutant strains

The construction of deletion mutants was performed as previously described.[42] The primers used are listed in Supplementary Table 1. Briefly, for in-frame mutant Δ*tssI2* and Δ*tssI2-tsiI2*, 600-bp sequences upstream and downstream of each target were cloned into pWM91, constructs were inserted into *V. fluvialis*

85003 via conjugation with SM10λ*pir E. coli*. Transconjugants were selected on LB agar plates containing ampicillin and streptomycin and were counter-selected by growing them on LB agar containing no salt and 10% (w/v) sucrose. The mutants were identified by PCR and confirmed by DNA sequencing and listed in Table 1

Site-directed mutagenesis of TssI2 C-terminal

Site-directed mutagenesis was performed by overlapping PCR using pSec-TssI2$^{834-1012}$-His plasmid as the template. All primers used are listed in Supplementary Table 1. The resultant fragments were cloned at *Nde*I/*Xho*I site in pSRKGm before the transformation of DH5α. All the constructs were confirmed by DNA sequencing and listed in Table 1.

Subcellular localization of TsiI2 protein

Subcellular fractions were extracted based on the cold osmotic shock procedure.[63,64] Briefly, *V. fluvialis* Δ*tssI2-tsiI2* harboring pMAL-TsiI2-

Myc was grown in 40 ml LB broth for 3 h to an OD_{600} of 0.5 and induced for 5 h with 200 μM of IPTG. The cells were harvested by centrifugation at $7,500 \times g$ for 10 min at 4°C. Cell pellet was washed twice with LB, resuspended in 1 ml of osmotic shock buffer (50 mM Tris-HCl pH 7.4, 20% sucrose, 10 mM EDTA, and protease inhibitor), incubated at 30°C for 10 min and then a 100 μl aliquot was collected for analysis of the whole-cell fraction. The remaining cells were recovered by centrifugation ($7,500 \times g$, 10 min at 4°C) and resuspended in 1 ml of ice-cold water and incubated on ice for 10 min for release of the periplasm. Samples were subjected to centrifugation ($9,000 \times g$, 10 min at 4°C), 100 μl of the resulting supernatant was collected for analysis of the periplasm fraction. The remaining samples were centrifuged again ($15,000 \times g$, 10 min at 4°C) and pellet was resuspended in 900 μl of 50 mM Tris-HCl pH 7.8 and 100 μl aliquot was retained for analysis of the cytoplasm and membrane fraction. Ten microliter of each fraction were separated by SDS-PAGE and subjected to immunoblotting with anti-maltose binding protein (MBP) (New England Bio-Labs #E8032L), anti-*E. coli* Crp (BioLegend, 664304) and anti-c-Myc (*ProteinFind*®, TransGen Biotech, HT101-01) antibodies.

Bacterial competition assay

Attacker (Sm^r) and prey (Rfp^r) strains were grown overnight in LB broth with proper antibiotics addition when maintenance of plasmids was required. Competition assays were performed as previously described.[42] Briefly, cultures were normalized to 1.5 McF and were mixed at a 9:1 ratio (attacker:prey). Triplicates of mixtures were incubated for 5 h or 12 h at 30°C on LB agar plates or LB plates containing 0.5 mM IPTG (when required to induce expression from plasmids). CFU of prey was calculated after they were grown on selective plates for 0 and 5 h or 12 h. Assays were repeated at least three times, and the results from representative experiments were shown.

Bacterial toxicity assay

To assess the toxicities of effector TssI2 or its truncated mutants or alanine substitution mutants,

E. coli MG1655 was transformed with the indicated pSRKGm-based IPTG-inducible expression vectors. *E. coli* transformants were normalized to 3.5 McF and diluted 100-fold in 5 ml LB broth supplemented with proper antibiotics when necessary. Cultures were grown at 37°C for 1 h and then induced or not induced at 37°C for 2 h. CFUs were enumerated at 0 h (T0) and 2 h (T2) after induction. Assays were repeated at least three times with similar results. To investigate immunity protection against effectors, we transformed pBAD24 or pBAD33-based recombinant plasmids harboring His-tagged effectors or Myc-tagged immunity into *E. coli* BL21(DE3). *E. coli* transformants were normalized to 2.0 McF and serially diluted. The dilutions were spotted on LB agar containing inducer (0.2% L-arabinose) or repressor (0.2% D-glucose). The images were acquired after 24 h. The experiment was repeated at least two times with similar results.

Bacterial adenylate cyclase-based two-hybrid (BACTH) assay

The BACTH system kit was used.[65] Briefly, the indicated proteins were fused to either the T18 or T25 fragments of CyaA in BACTH vectors and stored in *E. coli* K12 recA strains (XL1-Blue), and then the recombinant plasmids were transformed into the *E. coli* BTH101 reporter strain. Transformants were plated on LB agar plates supplemented with appropriate antibiotics, bromo-chloro-indolyl-galactopyranoside (X-gal, 40 mg/ml), IPTG (1 mM), and incubated for 24 h at 30°C. The experiment was repeated three times with similar results. Results from a representative experiment were shown.

Protein pull-down assay

Overnight cultures of *E. coli* BL21(DE3) containing plasmids for IPTG-inducible expression of the indicated 6xHis-tagged TssI2, $TssI2^{834-1012}$, or $VgrG3^{727-1017}$ and the Myc-tagged $TsiI2^{19-127}$ (the immunity protein was removed the Sec fragment (residue 1–18) to accumulate immunity fusion protein insides the cells) were diluted 100-fold in 200 ml LB broth supplemented with gentamicin and ampicillin and incubated at 37°C with agitation (200 rpm). Protein expression was induced by

adding 0.5 mM IPTG and 0.2% (w/v) L-arabinose when cultures reached an OD_{600} of 0.5, followed by incubation at 30°C for 4 h with agitation (200 rpm). Cells were harvested by centrifugation and then resuspended in 5 ml binding buffer (50 mM Tris-HCl, pH 7.5, and 150 mM NaCl, 2% (v/v) glycerol). The solution was sonicated five times with a 10s pulse, and cell debris was removed by centrifugation for 10 min at 12,000 × g at 4°C. Then, 100 μl of cleared supernatant was mixed with 25 μl of 5× SDS loading buffer, boiled at 100°C for 10 min, and kept for subsequent input protein analysis. In the following, 1 ml cleared supernatant was mixed with 100 μl HisPur^{TM} Ni-NTA resin (Thermo, 88221) and incubated overnight at 4°C with constant rotation. The resin was collected by centrifugation at 1000 × g at 4°C and washed with 1 ml binding buffer for three times, and resuspended with 100 μl of 1× SDS loading buffer, boiled at 100°C for 5 min, and kept for output protein analysis. The resin-bound proteins were analyzed by Western blotting using anti-His mAb (ZSGB-Bio, TA-02) or anti-c-Myc antibody (*ProteinFind*®, TransGen Biotech, HT101-01). The experiment was repeated at least two times with similar results, and the representative results were shown.

Western blot analysis

Western blotting was performed as described previously.[42] Briefly, the protein samples were separated by SDS-PAGE (12%), transferred onto PVDF membranes, and analyzed using specific primary antibodies as required, including anti-His monoclonal antibody (ZSGB-Bio, TA-02), anti-c-Myc antibody (*ProteinFind*®, TransGen Biotech, HT101-01), anti-*E. coli* Crp antibody (BioLegend, 664304) and anti-Hcp antisera.[42] Each immunoblot experiment was repeated at least two times.

Protein purification

The complete open reading frame of *tssI2* and the coding sequence of TsiI2 residues 19–127 were amplified and cloned into pET-30a(+) expression vector to construct recombinant plasmids pET30a-TssI2 and pET30a-TsiI2$^{19-127}$, respectively. *E. coli* BL21(DE3)pLysS containing pET30a-TssI2 or pET30a-TsiI2$^{19-127}$ was grown in LB broth at 37°C for 3 h, then shifted to 16°C, induced by 0.5 mM IPTG overnight. The cells were harvested by centrifugation (5,500 × g, 5 min at 4°C). Cell pellets were resuspended in a binding buffer (15 mM Tris-HCl, 500 mM NaCl), lysed by sonication, and centrifuged again (10,000 × g, 30 min at 4°C) to remove cellular pellets. The 6xHis-tagged TssI2 or TsiI2$^{19-127}$ in the supernatant was purified with the His•Bind® Purification Kit (Novegen, 70239–3). The target protein was rinsed with washing buffer (binding buffer supplemented with 20 mM imidazole (pH 8.0)) three times and eluted by elution buffer (binding buffer supplemented with 250 mM imidazole (pH 8.0)), and the solution was replaced with PBS. Protein purity was checked by SDS-PAGE and Coomassie blue staining. Protein concentrations were determined using the BCA assay and stored at −80°C.

The sequence of TssI2 N-terminal residues 1–833 and the sequence of C-terminal residues 834–1012 containing the site directed mutations were, respectively, amplified and cloned into the pET30a (+) vector to generate TssI2 variant constructs by using the pEASY®-Basic Seamless Cloning and Assembly Kit (Transgen Biotech, CU201-03). TssI2 variants with specific amino acid substitutions at the Pst domain were induced and purified as described above. The primers used are listed in Supplementary Table 1, and the constructs were confirmed by DNA sequencing and listed in Table 1.

Isothermal titration calorimetry

ITC was performed to analyze the binding affinity between TssI2 and TsiI2 with the use of the MicroCal iTC$_{200}$ instrument (GE Healthcare). The 6xHis-tagged TssI2 and TsiI2$^{19-127}$ proteins were purified as described above and prepared by dialysis in the PBS buffer (pH7.4). Protein concentrations were measured using the BCA Protein Assay Kit (TAKARA, T9300A) and were diluted to a concentration of 15 μM for TssI2 and 210 μM for TsiI2 protein. TsiI2 was filled into the syringe compartment while TssI2 was dispensed into the microcalorimetric cell. After temperature equilibration to 25°C, 3 μl of TsiI2 was titrated every 6 s into the TssI2-containing cell with a 150 s delay between each

injection under constant stirring. The titration heat was calculated to eliminate the effect of heat generated from titrating TsiI2 into PBS buffer. Data were analyzed using MicroCal-enabled Origin™ software (OriginLabs), and the thermal data were fitted to One Set of Sites binding model with a fixed N value of 1 to calculate the value of the equilibrium dissociation constant (K_d).

Lysozyme activity detection

Lysozyme activity was detected with fluorescence-labeled *M. lysodeikticus* cell walls by the EnzChek Lysozyme Assay Kit (Invitrogen, E-22013) according to the manufacturer's instructions. Samples were incubated with the above substrate in a 96-well microtiter plate (Thermo Fisher Scientific, 2605) at 37°C for 1 h or longer, protected from light. Fluorescence increment was measured with an excitation wavelength of 485 nm and an emission wavelength of 530 nm by a microplate reader (Infinite M200 Pro, Tecan). Background fluorescence without sample was subtracted from each value.

Lysis Assay

The cell lysis effects of TssI2 and its variants were tested as described elsewhere.[23,57] HEWL was used as a positive control. Briefly, mid-log cultures of *E. coli* MG1655 were harvested and suspended in PBS buffer (pH 7.4) to an OD_{600} of ~0.5. Aliquots of 100 μl were transferred to a Bioscreen Honeycomb 100-well plate, and the OD_{600} at 0 min was measured using Bioscreen C MBR (Growth Curves Ltd, Finland). A volume of 5 μl of PBS or 2 mg/ml of HEWL, TssI2, or its variant proteins was added to wells, followed immediately by the addition of 1 μl of 4 mg/ml of polymyxin B. The plate was incubated at 37°C in Bioscreen C MBR machine and the turbidity at OD_{600} was monitored at five-minute intervals for totally 50 minutes.

PG hydrolase assay and UPLC-MS analysis

PG isolation, hydrolase assay, and UPLC-MS analysis were conducted as described previously with some modifications.[57,66] Briefly, MG1655 were cultured to a stationary phase, and the cells were collected by centrifugation and resuspended in PBS buffer (pH 7.4). Cell lysis was achieved by adding the cell suspension dropwise to an equal volume of boiling 5% (w/v) SDS in tubes with stirring bar, inside a beaker of boiling water on a magnetic hot stirrer. The samples were boiled for an additional 1.5 h and stirred overnight at room temperature. Cell sacculi were collected by centrifugation for 40 min at 150,000 × g at 20°C and washed thoroughly with distilled water to remove SDS and then treated with Pronase E (1 mg/ml) overnight at 56°C to remove PG-associated proteins. The reaction was stopped by boiling it in SDS for 5 min. Purified peptidoglycan was washed four more times with distilled water and then suspended to a final wet weight concentration of 300 mg/ml.

For *in vitro* hydrolase assay, reactions were carried out in 10 mM NaAc buffer (pH 4.9) containing 10 mM NaCl, 3 mM $MgCl_2$ and 0.1% Triton X-100. 100 mg/ml (wet weight concentration) of purified PG was incubated with 5 μl of reaction buffer or 1 mg/ml HEWL, TssI2, or its variant proteins in a final volume of 105 μl. The turbidity at OD_{600} was monitored at five-minute intervals for totally 50 minutes at 30°C.

For the UPLC-MS analysis, the above hydrolase reaction mixtures were incubated overnight at 37°C. Following incubation, the reactions were terminated by boiling at 100°C for 5 min, and the insoluble debris was removed by centrifugation at 12,000 × g for 5 min. The muropeptide-containing supernatant was adjusted to pH 8.5–9.0 with 0.5 M borate buffer (pH 9.0) and then reduced with freshly prepared 2 M $NaBH_4$ for 30 min at room temperature. The samples were adjusted to pH 3.0 with 25% (v/v) orthophosphoric acid and filtered using 4 mm syringe filters (PVDF membrane, 0.22 μm pore size). The filtered samples were applied UPLC-MS analysis on the Agilent 1290 Infinity LC/6530 Q-TOF MS System. A Kinetex C18 UPLC column (2.6 μm particle size, 100 Å pore size, 10 × 2.1 mm) was used to separate individual muropeptides (detection wavelength of 204 nm) with mobile phase A (deionized water, 0.1% (v/v) formic acid) and mobile phase B (acetonitrile, 0.1% (v/v) formic acid). The injection volume was 10 μl. The column temperature was set at 45°C, and the flow rate was 0.2 ml/min.

The separation was achieved using the following gradient: 2–2.8% B at 0–2 min; 2.8–7.2% B at 2–5 min; 7.2–20% B at 5–13 min. The composition was then held at 20% B for 1 min and returned to initial conditions and maintained for 3 min for equilibration. The MS conditions were as follows: Peak identification was performed in positive mode, nitrogen gas nebulization was set at 35 psi with a flow of 5 l/min at 325°C while the sheath gas was set at 9 l/min at 325°C. The capillary and nozzle voltages were set at 3.5 kV and 1 kV, respectively. A complete mass scan ranging from m/z 300 to 1200 was used. Compounds of the unknown peaks were analyzed and identified from the relative retention time and mass-to-charge ratio[67] using Agilent MassHunter Qualitative Analysis software.

PSI-BLAST search for TssI2 C-terminal domain

Position-Specific Iterated BLAST was used to search homologous sequences containing TssI2 C-terminal domain, namely, the amino acid residues 834–1012 of TssI2. Nine iterations of PSI-BLAST were performed against the non-redundant protein sequence database. A maximum of 5000 hits was used, and the expected value threshold was set to 10^{-6} in each iteration. The proteins containing the TssI2 C-terminal domain were identified, and their sequences and feature tables were downloaded from NCBI on December 28–31, 2020. The results were filtered with 30% identity and 50% coverage and an E-value threshold of 10^{-9}. The result of taxonomy and domains of proteins were visualized using the SankeyMATIC software (http://sankeymatic.com/).

Identification of *V. fluvialis* containing VflT6SS2 locus

The amino acid sequence from TssB2 to RbsD (accession numbers KY319183) was employed to search VflT6SS2 locus against protein sequences in *V. fluvialis* genomes of the NCBI genome database by the BLASTp program. The e-value threshold was set to 10^{-5}. The results were filtered and merged by their serial number predicted by prodigal[68] and alignment start position, then manually inspected to identify the VflT6SS2 locus.

Other bioinformatics Analyses

The comparative analysis of VflT6SS2 locus in *V. fluvialis* 85003 and *V. cholerae* N16961 was performed using tBLASTn with an e-value of $1e^{-2}$ and the alignments of >1 kilobase (kb) were kept. The result was displayed by BlastViewer (https://github.com/dupengcheng/BlastViewer). Motif searching for *tssI2* and *tsiI2* was performed using the Pfam and NCBI-CDD databases.[45,69] An e-value of 0.01 was used. The tridimensional models were calculated by SWISS-MODEL servers and alphafold2[50] and validated using the SAVES server (https://saves.mbi.ucla.edu/), the highest score models were used in this study. The molecular docking of effector and immunity was analyzed through ZDOCK server v3.0.2 (http://zdock.umassmed.edu/). The multiple sequence alignments were constructed by Clustal Omega,[70] and the web logos were created by WebLogo 3 (http://weblogo.threeplusone.com/).[71] The structure figure of TssI2 and its homologs was prepared with IBS software.[72] Evolutionary analyses were conducted in MEGA X[73] from the amino acid sequences of TssI2 homologs, using the Maximum Likelihood method and Tamura-Nei model.[74] The tree presented is the consensus of 100 bootstrap repetitions.[75] GC content of the region from *tssM2-rbsD* was generated by the DNA Features Viewer 3.0.1 package in Python v.3.7.[76] The alignment of multiple amino acid sequences was displayed using ESPript 3.0 server.[77]

Statistical analysis

Data were statistically analyzed in the R programming environment, using the unpaired, two-tailed Student's t-test or ANOVA. $P < .05$ was considered statistically significant.

Disclosure statement

The authors declare that they have no competing interests.

Funding

Data Availability Statement

The authors confirm that the data supporting the findings of this study are available within the article and its supplementary materials.

References

1. Cianfanelli FR, Monlezun L, Coulthurst SJ. AIM, Load, Fire: the Type VI Secretion System, a Bacterial Nanoweapon. Trends Microbiol. 2016;24(1):51–62. doi:10.1016/j.tim.2015.10.005.

2. Pukatzki S, Ma AT, Sturtevant D, Krastins B, Sarracino D, Nelson WC, Heidelberg JF, Mekalanos JJ. Identification of a conserved bacterial protein secretion system in Vibrio cholerae using the Dictyostelium host model system. Proc Natl Acad Sci U S A. 2006 Jan 31;103 (5):1528–1533. doi:10.1073/pnas.0510322103.

3. Gerc AJ, Diepold A, Trunk K, Porter M, Rickman C, Armitage JP, Stanley-Wall NR, Coulthurst SJ. Visualization of the Serratia Type VI Secretion System Reveals Unprovoked Attacks and Dynamic Assembly. Cell Rep. 2015 Sep 29;12 (12):2131–2142. doi:10.1016/j.celrep.2015.08.053.

4. Records AR. The type VI secretion system: a multipurpose delivery system with a phage-like machinery. Mol Plant Microbe Interact. 2011;24 (7):751–757. doi:10.1094/MPMI-11-10-0262.

5. Aschtgen MS, Bernard CS, De Bentzmann S, Lloubès R, Cascales E. SciN is an outer membrane lipoprotein required for type VI secretion in enteroaggregative *Escherichia coli*. J Bacteriol. 2008;190(22):7523–7531. doi:10.1128/JB.00945-08.

6. Ma LS, Narberhaus F, Lai EM. IcmF Family Protein TssM Exhibits ATPase Activity and Energizes Type VI Secretion. Journal of Biological Chemistry. 2012;287 (19):15610–15621. doi:10.1074/jbc.M111.301630.

7. Felisberto-Rodrigues C, Durand E, Aschtgen MS, Blangy S, Ortiz-Lombardia M, Douzi B, Cambillau C, Cascales E. Towards a structural comprehension of bacterial type VI secretion systems: characterization of the TssJ-TssM complex of an *Escherichia coli* pathovar. PLoS Pathog. 2011 Nov;7(11):e1002386. doi:10.1371/journal.ppat.1002386.

8. Brunet YR, Zoued A, Boyer F, Douzi B, Cascales E. The Type VI Secretion TssEFGK-VgrG Phage-Like Baseplate Is Recruited to the TssJLM Membrane Complex via Multiple Contacts and Serves As Assembly Platform for Tail Tube/Sheath Polymerization. PLoS Genet. 2015;11(10):e1005545. doi:10.1371/journal.pgen.1005545.

9. Basler M, Pilhofer M, Henderson GP, Jensen GJ, Mekalanos JJ. Type VI secretion requires a dynamic contractile phage tail-like structure. Nature. 2012;483 (7388):182–186. doi:10.1038/nature10846.

10. Leiman PG, Basler M, Ramagopal UA, Bonanno JB, Sauder JM, Pukatzki S, Burley SK, Almo SC, Mekalanos JJ. Type VI secretion apparatus and phage tail-associated protein complexes share a common evolutionary origin. Proc Natl Acad Sci U S A. 2009 Mar 17;106(11):4154–4159. doi:10.1073/pnas.0813360106.

11. Brunet YR, Hénin J, Celia H, Cascales E. Type VI secretion and bacteriophage tail tubes share a common assembly pathway. EMBO Rep. 2014;15(3):315–321. doi:10.1002/embr.201337936.

12. Pell LG, Kanelis V, Donaldson LW, Howell PL, Davidson AR. The phage lambda major tail protein structure reveals a common evolution for long-tailed phages and the type VI bacterial secretion system. Proc Natl Acad Sci U S A. 2009;106(11):4160–4165. doi:10.1073/pnas.0900044106.

13. Pukatzki S, Ma AT, Revel AT, Sturtevant D, Mekalanos JJ. Type VI secretion system translocates a phage tail spike-like protein into target cells where it cross-links actin. Proc Natl Acad Sci USA. 2007;104 (39):15508–15513. doi:10.1073/pnas.0706532104.

14. Ho BT, Dong TG, Mekalanos JJ. A View to a Kill: the Bacterial Type VI Secretion System. Cell Host Microbe. 2014;15(1):9–21. doi:10.1016/j.chom.2013.11.008.

15. Trunk K, Peltier J, Liu YC, Dill BD, Walker L, Gow NAR, Stark MJR, Quinn J, Strahl H, Trost M, et al. The type VI secretion system deploys antifungal effectors against microbial competitors. Nat Microbiol. 2018 Aug;3 (8):920–931. doi:10.1038/s41564-018-0191-x.

16. Lin J, Zhang W, Cheng J, Yang X, Zhu K, Wang Y, Wei G, Qian PY, Luo ZQ, Shen X. A Pseudomonas T6SS effector recruits PQS-containing outer membrane vesicles for iron acquisition. Nat Commun. 2017 Mar 28;8:14888. doi:10.1038/ncomms14888.

17. Durand E, Cambillau C, Cascales E, Journet L. VgrG, Tae, Tle, and beyond: the versatile arsenal of Type VI secretion effectors. Trends Microbiol. 2014;22 (9):498–507. doi:10.1016/j.tim.2014.06.004.

18. Shneider MM, Buth SA, Ho BT, Basler M, Mekalanos JJ, Leiman PG. PAAR-repeat proteins sharpen and diversify the type VI secretion system spike. Nature. 2013;500(7462):350–353. doi:10.1038/nature12453.

19. Liang X, Moore R, Wilton M, Wong MJQ, Lam L, Dong TG. Identification of divergent type VI

secretion effectors using a conserved chaperone domain. Proc Natl Acad Sci USA. 2015;112 (29):9106–9111. doi:10.1073/pnas.1505317112.

20. Liu Y, Zhang Z, Wang F, Li DD, Li YZ. Identification of type VI secretion system toxic effectors using adaptors as markers. Comput Struct Biotechnol J. 2020;18:3723–3733. doi:10.1016/j.csbj.2020.11.003.

21. Ma J, Sun M, Dong W, Pan Z, Lu C, Yao H. PAAR-Rhs proteins harbor various C-terminal toxins to diversify the antibacterial pathways of type VI secretion systems. Environ Microbiol. 2017;19(1):345–360. doi:10.1111/1462-2920.13621.

22. Berni B, Soscia C, Djermoun S, Ize B, Bleves S. A Type VI Secretion System Trans-Kingdom Effector Is Required for the Delivery of a Novel Antibacterial Toxin in *Pseudomonas aeruginosa*. Front Microbiol. 2019;10:1218. doi:10.3389/fmicb.2019.01218.

23. Brooks TM, Unterweger D, Bachmann V, Kostiuk B, Pukatzki S. Lytic activity of the Vibrio cholerae type VI secretion toxin VgrG-3 is inhibited by the antitoxin TsaB. J Biol Chem. 2013;288(11):7618–7625. doi:10.1074/jbc.M112.436725.

24. Ma AT, Mekalanos JJ. In vivo actin cross-linking induced by Vibrio cholerae type VI secretion system is associated with intestinal inflammation. Proc Natl Acad Sci U S A. 2010;107(9):4365–4370. doi:10.1073/pnas.0915156107.

25. Ma J, Pan Z, Huang J, Sun M, Lu C, Yao H. The Hcp proteins fused with diverse extended-toxin domains represent a novel pattern of antibacterial effectors in type VI secretion systems. Virulence. 2017;8 (7):1189–1202. doi:10.1080/21505594.2017.1279374.

26. Coulthurst S. The Type VI secretion system: a versatile bacterial weapon. Microbiology (Reading, Engl). Published Online March. 2019:20. doi:10.1099/mic.0.000789.

27. Filloux A, Hachani A, Bleves S. The bacterial type VI secretion machine: yet another player for protein transport across membranes. Microbiology. 2008;154 (6):1570–1583. doi:10.1099/mic.0.2008/016840-0.

28. Whitney JC, Chou S, Russell AB, Biboy J, Gardiner TE, Ferrin MA, Brittnacher M, Vollmer W, Mougous JD. Identification, structure, and function of a novel type VI secretion peptidoglycan glycoside hydrolase effector-immunity pair. J Biol Chem. 2013 Sep 13;288 (37):26616–26624. doi:10.1074/jbc.M113.488320.

29. Bondage DD, Lin JS, Ma LS, Kuo CH, Lai EM. VgrG C terminus confers the type VI effector transport specificity and is required for binding with PAAR and adaptor-effector complex. Proc Natl Acad Sci U S A. 2016;113(27):E3931–3940. doi:10.1073/pnas.1600428113.

30. Flaugnatti N, Le TT, Canaan S, Aschtgen MS, Nguyen VS, Blangy S, Kellenberger C, Roussel A, Cambillau C, Cascales E, et al. A phospholipase A1 antibacterial Type VI secretion effector interacts directly with the C-terminal domain of the VgrG spike

protein for delivery. Mol Microbiol. 2016 Mar;99 (6):1099–1118. doi:10.1111/mmi.13292.

31. Flaugnatti N, Rapisarda C, Rey M, Beauvois SG, Nguyen VA, Canaan S, Durand E, Chamot-Rooke J, Cascales E, Fronzes R, et al. Structural basis for loading and inhibition of a bacterial T6SS phospholipase effector by the VgrG spike. EMBO J. 2020 Jun 2;39(11): e104129. doi:10.15252/embj.2019104129.

32. Dong TG, Ho BT, Yoder-Himes DR, Mekalanos JJ. Identification of T6SS-dependent effector and immunity proteins by Tn-seq in Vibrio cholerae. Proc Natl Acad Sci U S A. 2013 Feb 12;110(7):2623–2628. doi:10.1073/pnas.1222783110.

33. Liang X, Pei TT, Wang ZH, Xiong W, Wu LL, Xu P, Lin S, Dong TG. Characterization of Lysozyme-Like Effector TseP Reveals the Dependence of Type VI Secretion System (T6SS) Secretion on Effectors in Aeromonas dhakensis Strain SSU. Appl Environ Microbiol. 2021 May 26;87(12):e0043521. doi:10.1128/AEM.00435-21.

34. Ma LS, Hachani A, Lin JS, Filloux A, Lai EM. Agrobacterium tumefaciens deploys a superfamily of type VI secretion DNase effectors as weapons for interbacterial competition in planta. Cell Host Microbe. 2014;16(1):94–104. doi:10.1016/j.chom.2014.06.002.

35. Russell AB, LeRoux M, Hathazi K, Agnello DM, Ishikawa T, Wiggins PA, Wai SN, Mougous JD. Diverse type VI secretion phospholipases are functionally plastic antibacterial effectors. Nature. 2013 Apr 25;496(7446):508–512. doi:10.1038/nature12074.

36. Hernandez RE, Gallegos-Monterrosa R, Coulthurst SJ. Type VI secretion system effector proteins: effective weapons for bacterial competitiveness. Cell Microbiol. 2020 Sep;22(9):e13241. doi:10.1111/cmi.13241.

37. Ramamurthy T, Chowdhury G, Pazhani GP, Shinoda S. Vibrio fluvialis: an emerging human pathogen. Front Microbiol. 2014;5. doi:10.3389/fmicb.2014.00091.

38. Igbinosa EO, Okoh AI. Vibrio fluvialis: an unusual enteric pathogen of increasing public health concern. Int J Environ Res Public Health. 2010;7(10):3628–3643. doi:10.3390/ijerph7103628.

39. Chowdhury G, Pazhani GP, Sarkar A, Rajendran K, Mukhopadhyay AK, Bhattacharya MK, Ghosh A, Ramamurthy T. Carbapenem Resistance in Clonally Distinct Clinical Strains of Vibrio fluvialis Isolated from Diarrheal Samples. Emerg Infect Dis. 2016 Oct;22(10):1754–1761. doi:10.3201/eid2210.151612.

40. Liang P, Cui X, Du X, Kan B, Liang W. The virulence phenotypes and molecular epidemiological characteristics of Vibrio fluvialis in China. Gut Pathog. 2013;5(1):6. doi:10.1186/1757-4749-5-6.

41. Chowdhury G, Ramamurthy T, Ghosh A, Dutta S, Takahashi E, Mukhopadhyay AK. Emergence of Azithromycin Resistance Mediated by Phosphotransferase-Encoding mph(A) in Diarrheagenic Vibrio fluvialis. mSphere. 2019;4(3). doi:10.1128/mSphere.00215-19.

42. Huang Y, Du P, Zhao M, Liu W, Du Y, Diao B, Li J, Kan B, Liang W. Functional Characterization and Conditional Regulation of the Type VI Secretion System in Vibrio fluvialis. Front Microbiol. 2017 Mar 30;8:528. doi:10.3389/fmicb.2017.00528.

43. Pan J, Zhao M, Huang Y, Li J, Liu X, Ren Z, Kan B, Liang W. Integration Host Factor Modulates the Expression and Function of T6SS2 in Vibrio fluvialis. Front Microbiol. 2018 May 15;9:962. doi:10.3389/fmicb.2018.00962.

44. Liu X, Pan J, Gao H, Han Y, Zhang A, Huang Y, Liu P, Kan B, Liang W. CqsA/LuxS-HapR Quorum sensing circuit modulates type VI secretion system VflT6SS2 in Vibrio fluvialis. Emerg Microbes Infect. 2021 Dec;10(1):589–601. doi:10.1080/22221751.2021.1902244.

45. Mistry J, Chuguransky S, Williams L, Qureshi M, Salazar GA, Sonnhammer ELL, Tosatto SCE, Paladin L, Raj S, Richardson LJ, et al. Pfam: the protein families database in 2021. Nucleic Acids Res. 2021 Jan 8;49(D1):D412–D419. doi:10.1093/nar/gkaa913.

46. Waterhouse A, Bertoni M, Bienert S, Studer G, Tauriello G, Gumienny R, Heer FT, de Beer TAP, Rempfer C, Bordoli L, et al. Swiss-MODEL: homology modelling of protein structures and complexes. Nucleic Acids Res. 2018 Jul 2;46(W1):W296–W303. doi:10.1093/nar/gky427.

47. Vollmer W, Pilsl H, Hantke K, Höltje JV, Braun V. Pesticin displays muramidase activity. J Bacteriol. 1997;179(5):1580–1583. doi:10.1128/jb.179.5.1580-1583.1997.

48. Storey D, McNally A, Åstrand M, Sa-Pessoa Graca Santos J, Rodriguez-Escudero I, Elmore B, Palacios L, Marshall H, Hobley L, Molina M, et al. Klebsiella pneumoniae type VI secretion system-mediated microbial competition is PhoPQ controlled and reactive oxygen species dependent. PLoS Pathog. 2020 Mar 19;16(3):e1007969. doi:10.1371/journal.ppat.1007969.

49. Karimova G, Pidoux J, Ullmann A, Ladant D. A bacterial two-hybrid system based on a reconstituted signal transduction pathway. Proc Natl Acad Sci U S A. 1998 May 12;95(10):5752–5756. doi:10.1073/pnas.95.10.5752.

50. Mirdita M, Schütze K, Moriwaki Y, Heo L, Ovchinnikov S, Steinegger M. ColabFold: making protein folding accessible to all. Nat Methods. 2022 Jun;19(6):679–682. doi:10.1038/s41592-022-01488-1.

51. Pierce BG, Wiehe K, Hwang H, Kim BH, Vreven T, Weng Z. ZDOCK server: interactive docking prediction of protein-protein complexes and symmetric multimers. Bioinformatics. 2014;30(12):1771–1773. doi:10.1093/bioinformatics/btu097.

52. Patzer SI, Albrecht R, Braun V, Zeth K. Structural and mechanistic studies of pesticin, a bacterial homolog of phage lysozymes. J Biol Chem. 2012;287(28):23381–23396. doi:10.1074/jbc.M112.362913.

53. Tian W, Chen C, Lei X, Zhao J, Liang J. CASTp 3.0: computed atlas of surface topography of proteins. Nucleic Acids Res. 2018;46(W1):W363–W367. doi:10.1093/nar/gky473.

54. Ho BT, Fu Y, Dong TG, Mekalanos JJ. Vibrio cholerae type 6 secretion system effector trafficking in target bacterial cells. Proc Natl Acad Sci U S A. 2017;114(35):9427–9432. doi:10.1073/pnas.1711219114.

55. Russell AB, Singh P, Brittnacher M, Bui NK, Hood RD, Carl MA, Agnello DM, Schwarz S, Goodlett DR, Vollmer W, et al. A widespread bacterial type VI secretion effector superfamily identified using a heuristic approach. Cell Host Microbe. 2012 May 17;11(5):538–549. doi:10.1016/j.chom.2012.04.007.

56. Hersch SJ, Watanabe N, Stietz MS, Manera K, Kamal F, Burkinshaw B, Lam L, Pun A, Li M, Savchenko A, et al. Envelope stress responses defend against type six secretion system attacks independently of immunity proteins. Nat Microbiol. 2020 May;5(5):706–714. doi:10.1038/s41564-020-0672-6.

57. Wood TE, Howard SA, Förster A, Nolan LM, Manoli E, Bullen NP, Yau HCL, Hachani A, Hayward RD, Whitney JC, et al. The Pseudomonas aeruginosa T6SS Delivers a Periplasmic Toxin that Disrupts Bacterial Cell Morphology. Cell Rep. 2019 Oct 1;29(1):187–201.e7. doi:10.1016/j.celrep.2019.08.094.

58. Ruhe ZC, Low DA, Hayes CS. Polymorphic Toxins and Their Immunity Proteins: diversity, Evolution, and Mechanisms of Delivery. Annu Rev Microbiol. 2020;74(1):497–520. doi:10.1146/annurev-micro-020518-115638.

59. Ross BD, Verster AJ, Radey MC, Schmidtke DT, Pope CE, Hoffman LR, Hajjar AM, Peterson SB, Borenstein E, Mougous JD. Human gut bacteria contain acquired interbacterial defence systems. Nature. 2019 Nov;575(7781):224–228. doi:10.1038/s41586-019-1708-z.

60. Nterweger D, Miyata ST, Bachmann V, Brooks TM, Mullins T, Kostiuk B, Provenzano D, Pukatzki S. The Vibrio cholerae type VI secretion system employs diverse effector modules for intraspecific competition. Nat Commun. 2014 Apr 1;5:3549. doi:10.1038/ncomms4549.

61. Yildiz FH, Schoolnik GK. Role of rpoS in stress survival and virulence of Vibrio cholerae. J Bacteriol. 1998;180(4):773–784. doi:10.1128/JB.180.4.773-784.1998.

62. Liang W, Pascual-Montano A, Silva AJ, Benitez JA. The cyclic AMP receptor protein modulates quorum sensing, motility and multiple genes that affect intestinal colonization in Vibrio cholerae. Microbiology. 2007 Sep;153(Pt 9):2964–2975. doi:10.1099/mic.0.2007/006668-0.

63. English G, Trunk K, Rao VA, Srikannathasan V, Hunter WN, Coulthurst SJ. New secreted toxins and immunity proteins encoded within the Type VI secretion system gene cluster of Serratia marcescens. Mol

Microbiol. 2012;86(4):921–936. doi:10.1111/mmi.12028.

64. Sibinelli-Sousa S, Hespanhol JT, Nicastro GG, Matsuyama BY, Mesnage S, Patel A, de Souza RF, Guzzo CR, Bayer-Santos E. A Family of T6SS Antibacterial Effectors Related to l,d-Transpeptidases Targets the Peptidoglycan. Cell Rep. 2020 Jun 23;31 (12):107813. doi:10.1016/j.celrep.2020.107813.

65. Karimova G, Gauliard E, Davi M, Ouellette SP, Ladant D. Protein-Protein Interaction: bacterial Two-Hybrid. Methods Mol Biol. 2017;1615:159–176. doi:10.1007/978-1-4939-7033-9_13.

66. Alvarez L, Hernandez SB, de Pedro MA, Cava F. Ultra-Sensitive, High-Resolution Liquid Chromatography Methods for the High-Throughput Quantitative Analysis of Bacterial Cell Wall Chemistry and Structure. Methods Mol Biol. 2016;1440:11–27. doi:10.1007/978-1-4939-3676-2_2.

67. Bui NK, Gray J, Schwarz H, Schumann P, Blanot D, Vollmer W. The peptidoglycan sacculus of Myxococcus xanthus has unusual structural features and is degraded during glycerol-induced myxospore development. J Bacteriol. 2009;191(2):494–505. doi:10.1128/JB.00608-08.

68. Hyatt D, Chen GL, LoCascio PF, Land ML, Larimer FW, Hauser LJ. Prodigal: prokaryotic gene recognition and translation initiation site identification. BMC Bioinform. 2010;11(1):119. doi:10.1186/1471-2105-11-119.

69. Marchler-Bauer A, Lu S, Anderson JB, Chitsaz F, Derbyshire MK, DeWeese-Scott C, Fong JH, Geer LY, Geer RC, Gonzales NR, et al. CDD: a Conserved Domain Database for the functional annotation of proteins. Nucleic Acids Res. 2011 Jan;39:D225–9. doi:10.1093/nar/gkq1189.

70. Sievers F, Wilm A, Dineen D, Gibson TJ, Karplus K, Li W, Lopez R, McWilliam H, Remmert M, Söding J, et al. Fast, scalable generation of high-quality protein multiple sequence alignments using Clustal Omega. Mol Syst Biol. 2011 Oct 11;7:539. doi:10.1038/msb.2011.75.

71. Crooks GE, Hon G, Chandonia JM, Brenner SE. WebLogo: a sequence logo generator. Genome Res. 2004;14(6):1188–1190. doi:10.1101/gr.849004.

72. Liu W, Xie Y, Ma J, Luo X, Nie P, Zuo Z, Lahrmann U, Zhao Q, Zheng Y, Zhao Y, et al. IBS: an illustrator for the presentation and visualization of biological sequences. Bioinformatics. 2015 Oct 15;31 (20):3359–3361. doi:10.1093/bioinformatics/btv362.

73. Kumar S, Stecher G, Li M, Knyaz C, Tamura K. MEGA X: molecular Evolutionary Genetics Analysis across Computing Platforms. Mol Biol Evol. 2018 Jun 1;35 (6):1547–1549. doi:10.1093/molbev/msy096.

74. Tamura K, Nei M. Estimation of the number of nucleotide substitutions in the control region of mitochondrial DNA in humans and chimpanzees. Mol Biol Evol. 1993;10(3):512–526. doi:10.1093/oxfordjournals.molbev.a040023.

75. Felsenstein J. Phylogenies and the Comparative Method. Am Nat. 1985;125(1):1–15. doi:10.1086/284325.

76. Zulkower V, Rosser S. DNA Features Viewer: a sequence annotation formatting and plotting library for Python. Bioinformatics. 2020 Aug 1;36 (15):4350–4352. doi:10.1093/bioinformatics/btaa213.

77. Robert X, Gouet P. Deciphering key features in protein structures with the new ENDscript server. Nucleic Acids Res. 2014 Jul;42:W320–4. doi:10.1093/nar/gku316.